Physical mechanism of mind changes and tradeoffs among speed, accuracy, and energy cost in brain decision making: Landscape, flux, and path perspectives*

Han Yan(闫晗)[1,2], Kun Zhang(张坤)[2], and Jin Wang(汪劲)[1,2,3,†]

[1] College of Physics, Jilin University, Changchun 130012, China
[2] State Key Laboratory of Electroanalytical Chemistry, Changchun Institute of Applied Chemistry, Chinese Academy of Sciences, Changchun 130022, China
[3] Department of Chemistry and Physics, Stony Brook University, Stony Brook, NY 11794-3400, USA

(Received 20 January 2016; revised manuscript received 20 April 2016; published online 1 June 2016)

Cognitive behaviors are determined by underlying neural networks. Many brain functions, such as learning and memory, have been successfully described by attractor dynamics. For decision making in the brain, a quantitative description of global attractor landscapes has not yet been completely given. Here, we developed a theoretical framework to quantify the landscape associated with the steady state probability distributions and associated steady state curl flux, measuring the degree of non-equilibrium through the degree of detailed balance breaking for decision making. We quantified the decision-making processes with optimal paths from the undecided attractor states to the decided attractor states, which are identified as basins of attractions, on the landscape. Both landscape and flux determine the kinetic paths and speed. The kinetics and global stability of decision making are explored by quantifying the landscape topography through the barrier heights and the mean first passage time. Our theoretical predictions are in agreement with experimental observations: more errors occur under time pressure. We quantitatively explored two mechanisms of the speed-accuracy tradeoff with speed emphasis and further uncovered the tradeoffs among speed, accuracy, and energy cost. Our results imply that there is an optimal balance among speed, accuracy, and the energy cost in decision making. We uncovered the possible mechanisms of changes of mind and how mind changes improve performance in decision processes. Our landscape approach can help facilitate an understanding of the underlying physical mechanisms of cognitive processes and identify the key factors in the corresponding neural networks.

Keywords: decision making, non-equilibrium landscape and flux, speed-accuracy tradeoff, energy cost

PACS: 87.19.lj, 87.19.ll, 87.18.Vf, 05.10.-a **DOI:** 10.1088/1674-1056/25/7/078702

1. Introduction

The neural circuit as a dynamical system is the basis of cognitive function, including decision making.[1–4] We face different choices in our daily lives. Most decisions are made unconsciously. Sometimes we must first evaluate the costs and benefits of addressing the situations of risk or uncertainty before we make an optimal decision, choosing from a set of alternatives.[5–7] Understanding the mechanisms of decision making has been challenging. In recent years, researchers have made progress in both theoretical and experimental fields related to cognitive processes, such as decision making.[8–11]

The diffusion model was successful in describing behavior responses such as accuracy and the shape of response-time distributions in two-choice decision making tasks.[8,12] In the diffusion model, a decision variable evolves from a starting point until it reaches one of the two response boundaries corresponding to the two decisions, as the result of fluctuations. Although the diffusion model gives a good account of behavior data, some features observed in the experiments cannot be easily captured in the diffusion model. For example, the experimental observation that longer response times in error trials than in correct trails cannot be fitted by the diffusion model unless it is assumed that parameters of the model (the initial condition and the drift rate) vary across trials. In the delayed visual motion discrimination task, the monkey is required to hold the decision in the working memory for a few seconds.[13] The working memory, which is needed to account for the delayed response in this task cannot be easily explained in the diffusion model.

However, these features can be naturally explained in the biophysically motivated attractor model of a two-choice decision-making task,[14–16] where a decision is made when the system is attracted to one decided attractor associated with one of the two choices. The attractor dynamics have been shown to be successful in describing biological and cognitive processes.[3,17–23] In the attractor model, the working memory can be stored in the decided attractor even after the stimulus is removed. The dynamics of the attractor model are dominated by an attractor landscape in which the states correspond to activities of neural populations. Both behavioral and neurophysiological data in the decision-making process can be well

*Project supported by the National Natural Science Foundation of China (Grant Nos. 21190040, 91430217, and 11305176).
†Corresponding author. E-mail: jin.wang.1@stonybrook.edu
© 2016 Chinese Physical Society and IOP Publishing Ltd

described by such a model.[14–16] However, the attractor landscape introduced provides a qualitative concept, and further quantification is required.

Based on the advantages of the above models, Roxin and Ledberg made progress in relating the diffusion model to the neuronal activities by suggesting a general method to reduce multi-dimensional biophysical models to a one-dimensional nonlinear diffusion model.[11] This one-dimensional nonlinear diffusion model also provides an excellent fit to behavioral data in the two-choice decision-making tasks. Furthermore, an analytical form of energy function can be constructed, with a negative gradient serving as the driving force of the system. Although great efforts have been made to relate the diffusion model to biophysically realistic neural circuits, the detailed information of the complicated dynamical system consisting of a great number of neurons cannot be easily obtained from the one-dimensional diffusion model. The main purpose of our work is to explore the underlying mechanisms of the cognitive processes of decision making from the physical and quantitative perspectives.

In general, biophysics-based decision-making models can show more neurophysiological information such as the evolution of the average firing rates of neural populations and the sources of fluctuations.[14–16] Parameters in the model are directly related to biologically meaningful quantities, which provides us with a chance to explore the neuronal mechanisms of decision-making systems. However, the attractor landscape in the attractor model is not completely quantified. Although the position of each attractor state is shown, the relative weights of these states and the quantified attractor landscape are not given.[14–16] Quantifying the topology of the attractor landscape through the relative weights of states can account for the stability of the global system, particularly for the functional attractors. Previous works have shown better performances in easier decision tasks.[15,16] The underlying mechanisms determining the speed, accuracy, and changes of mind in the attractor model remain challenging to quantify. Furthermore, what should be noticed is that the realistic neural networks are always non-equilibrium systems due to the material, energy, and information exchanges with the environment. For the general non-equilibrium dynamical systems, the driving force of the dynamics cannot be written as a pure gradient of an energy landscape.[20–23]

In our previous works, we have developed a landscape and flux theory for general non-equilibrium dynamical systems.[20–25] The potential landscape we constructed is closely related to the steady-state probability distributions of the non-equilibrium systems. The probability density distributions of neuronal activity variables have been studied to explore the influences of fluctuations on decision-making behavior.[26,27] We found that the dynamics of the non-equilibrium systems are determined by both the underlying landscape and the curl probability flux. The flux, in addition to the gradient of the non-equilibrium landscape, is responsible for many characteristic non-equilibrium behaviors. For example, our previous studies showed that the flux provides the main driving force of oscillatory behaviors in neural networks.[23] Furthermore, as the result of the flux, the dominant kinetics path does not necessarily pass through the landscape saddles (local maximum) to get to the local minimum, and the forward and backward paths are irreversible.[22,24] Furthermore, we established the non-equilibrium thermodynamics, extending the equilibrium thermodynamics based on the landscape and flux theory.[23,24,28,30] The entropy production rate in the non-equilibrium systems is linked to the flux term, which originates from the energy pump from the environments.[29–31] Quantifying the entropy production rate or energy dissipation rate gives us new insights into the energy cost in non-equilibrium biological systems.

In this work, we applied the landscape and flux theory to a biophysics-based model to quantitatively investigate the nature of the decision-making process from a physical perspective. We quantified basins of attraction as the fates of decision-making with higher probabilities. The stability of basins of attraction corresponding to functional states was explored by quantifying the underlying potential landscape topography through the barrier heights and the kinetic transition times characterized by the mean first passage time between the basins of attraction. We also quantified the optimal path from the undecided state to the decided state with a path integral approach.[32] We found that both the landscape and flux determine the dynamical processes and the associated speed. Furthermore, we explored how the potential landscapes are influenced by the changes of the key factors of the underlying neural network. The underlying mechanism of the speed-accuracy tradeoff was quantitatively explored by varying the additional stimulus input and input threshold in this study, and both of them increase the baseline activity of the integrator neurons. Differently from previous works, here our quantifications of the decision time and accuracy performance avoid time-consuming calculations from the statistics of the data. Furthermore, we quantified the energy costs and explored the tradeoffs among speed, accuracy, and energy cost in decision-making. We found speed emphasis will cost more energy in unit time. However, a varying input threshold and additional input play different roles in regulating the total energy cost, which is defined as the entropy production rate multiplied by the decision time. If the input threshold is the main regulation mechanism, we showed that the total energy cost increases monotonously as the accuracy increases, and it decreases monotonously as the decision time decreases. When presenting additional stimulus input is the dominated mecha-

nism, the total energy cost in decision making changes non-monotonically as the additional input increases. Reasonable but suboptimal accuracy and performance can be achieved with optimal energy cost and speed. In other words, for decision making in this case, there is an optimal energy cost with a nearly optimal fast speed at an intermediate accuracy. We also explored the mechanism of changes of mind, and we suggested a physical explanation of the interesting phenomenon observed in the experiments. Above all, the novelty of our work lies in the global quantification of the dynamics and identifications of the driving force (landscape and curl flux), thermodynamics (energy cost), the underlying mechanisms of decision-making (processes quantified by the optimal paths and the speed of decision-making) and quantifications of the relations of speed, accuracy, energy cost, and changes of mind.

2. Models and methods

2.1. Non-equilibrium landscape theory for general neural networks

In realistic biological systems, there are always intrinsic and extrinsic fluctuations.[33] For neural circuits, fluctuating components of the inputs outside the circuits give the external fluctuations, and the statistical fluctuations within the circuit give the intrinsic fluctuations. Therefore, we should take the fluctuations into consideration when studying the dynamics of neural network systems. The underlying dynamics of neural network systems are generally non-linear and unpredictable, and chaos can emerge. The conventional way of exploring neural network dynamical systems by following the single trajectories of the time evolution of the system cannot easily capture the global properties of the systems. However, the probabilistic evolution is often linear and predictable, which can shape the global nature of the stochastic dynamics. Therefore, we focus on the probabilistic evolution of the system by solving the corresponding Fokker–Planck equations. We can obtain the steady state probability distribution $P_{\rm ss}$, which satisfies $\partial P_{\rm ss}/\partial t = 0$. Then, the probabilistic landscape can be quantified as $U = -\ln P_{\rm ss}$, where U is the quantified potential landscape and $P_{\rm ss}$ is the steady-state probability distribution.[20–23] Dynamical systems will be expected to be attracted to some states with higher probabilities and lower potentials in the temporal evolution processes because the weight of each state is inhomogeneously distributed in state space. The states with the locally highest probability represent attractor states which are typically related to biological functions.

Cognitive functions are achieved by the collective efforts of neural circuits rather than individual neurons. The potential landscape can provide a quantitative description of the global nature of neural networks rather than the local information from single trajectories.[20–23] To quantify the potential landscapes, we focus on the steady-state probability distributions. Here the noise term should be taken into account to capture the statistical properties. Because we start with the dynamical equations of the neural network, we can write the corresponding Langevin equations as: $z\mathrm{d}x_i/\mathrm{d}t = \boldsymbol{F}(\boldsymbol{x}) + \zeta$. Here we assume the noise is Gaussian distributed. The auto-correlation of the fluctuation is assumed to be $\langle \zeta_i(t)\zeta_j(t')\rangle = 2\boldsymbol{D}\delta(t-t')$, $\boldsymbol{D}$ is the diffusion coefficient tensor (matrix) measuring the strength of the fluctuations. The probability evolution can be quantified by solving the corresponding Fokker–Plank equation: $\partial P(\boldsymbol{x},t)/\partial t = -\boldsymbol{\nabla}\cdot\boldsymbol{J}$, where $\boldsymbol{J}$ is the probability flux defined as $\boldsymbol{J} = \boldsymbol{F}(\boldsymbol{x})P(\boldsymbol{x},t) - \boldsymbol{D}\boldsymbol{\nabla}P(\boldsymbol{x},t)$. The Fokker–Planck equation can be interpreted as local probability conservation, where the local probability change is determined by the inward or outward flux. Here, we take $\boldsymbol{D}$ as a constant diffusion tensor independent of underlying variables. The steady-state probability distribution satisfies $\partial P_{\rm ss}(\boldsymbol{x},t)/\partial t = -\boldsymbol{\nabla}\cdot\boldsymbol{J}_{\rm ss} = 0$. Finally, the potential landscape U can be quantified by the steady-state probability ($P_{\rm ss}$) $U = -\ln P_{\rm ss}$.[20,21,32,34] The driving force of the dynamics can be decomposed into a gradient of the potential landscape and steady state curl flux force as: $\boldsymbol{F} = -\boldsymbol{D}\boldsymbol{\nabla}\boldsymbol{U} + \boldsymbol{J}_{\rm ss}/\boldsymbol{P}_{\rm ss}$. When the steady state flux is zero, there is no net flux flow in or out; the system is in a detailed balance. When the flux is not zero, there is a net steady state flux flowing around. This breaks the detailed balance and measures how far away the system is from the equilibrium. Because the steady-state flux satisfies the curl free condition ($\boldsymbol{\nabla}\cdot\boldsymbol{J}_{\rm ss} = 0$), the flux is rotational or curl. Whereas the landscape provides a gradient driving force, the flux provides a curl driving force for the dynamics.

2.2. Reduced two-population neural network model

We have introduced our non-equilibrium landscape and flux theory for general networks. Here we applied this theory to a simplified biophysics-based model that could account for the experimental results in decision-making processes.[15,16] This simplified model is a reduced version of the neural network model with thousands of spiking neurons that interact with each other. With a mean-field approach, the dynamics of a neural population can be represented by a single unit. The mean activity (firing rate) of a neural population depends on the synaptic input currents. The input current is a function of synaptic gating variables, which represents the fraction of the activated synaptic conductance. Furthermore, a third inhibitory neural population through which the two excitatory neural pools inhibit each other is neglected for simplicity. Then the dynamics of the decision-making neural network model can be represented by the dynamics of two excitatory neural populations. The details of model reduction can be found in a previous paper.[15]

As shown in Fig. 1(a), this reduced model consists of two competing neural pools that are selective for the leftward or

rightward direction of decision making, respectively. Within each pool of neurons, there are strong recurrent excitatory connections that are dominated by NMDA-mediated receptors. Since the time constant of NMDA synaptic gating variables is much slower than the time constant of firing rate r. The dynamical evolution of firing rates (quickly reaching the steady state values) can be neglected compared with the slower change of the NMDA gating variables. Firing rate r_i of neural population i as a function of total synaptic input current $I_{i,\mathrm{tot}}$ can be written as

$$r_i = f(I_{i,\mathrm{tot}}) = \frac{aI_{i,\mathrm{tot}} - b}{1 - \exp[-d(aI_{i,\mathrm{tot}} - b)]}, \quad i = 1,2, \tag{1}$$

where the input–output function parameter values are $a = 269.5\ (\mathrm{VnC})^{-1}$, $b = 108$ Hz, and $d = 0.154$ s.[15] The contributions of AMPA receptors to the total synaptic currents inside the circuit can be also neglected. Then the dynamics of the network is dominated by the gating variable S_i. The model can be described by the following dynamical equations:

$$\frac{\mathrm{d}S_i}{\mathrm{d}t} = -\frac{S_i}{\tau_S} + (1 - S_i)\gamma f(I_{i,\mathrm{tot}}), \quad i = 1,2. \tag{2}$$

According to the above equations, the average gating variables S_i at the steady state are positively correlated with the average firing rates of neural population 1,2. Therefore, the gating variables S_i also reflect the mean activity of the neural population. The total synaptic input currents of the two neural populations dominated by the NMDA receptors are

$$I_{1,\mathrm{tot}} = J_{11}S_1 - J_{12}S_2 + I_0 + I_{\mathrm{motion},1}, \tag{3}$$

$$I_{2,\mathrm{tot}} = J_{22}S_2 - J_{21}S_1 + I_0 + I_{\mathrm{motion},2}. \tag{4}$$

Here the NMDA synaptic couplings are $J_{11} = J_{22} = 0.2609$ nA and $J_{12} = J_{21} = 0.0497$ nA, and $I_0 = 0.3255$ nA is the average background synaptic input. Also, $\gamma = 60$ ms and $\tau_S = 100$ ms. The particular values of the parameters in the model here are the same as the ones shown in the previous work.[15] These two neural groups are self-activated and mutually inhibited with each other. The competition between these two excitatory neural populations is determined by the sensory input.

Random dot motion (RDM) tasks were designed to study decision-making behavior.[13,35–37] Monkeys are asked to watch the random dot motion and make a decision by saccadic eye movement. Here we use $I_{\mathrm{motion},i}$ as the external sensory input to selective neural population i corresponding to the random dot stimulus current in RDM tasks. It can be written as: $I_{\mathrm{motion},i} = J_{\mathrm{A,ext}}\mu_0(1 \pm c'/100\%)$, where $J_{\mathrm{A,ext}} = 5.2 \times 10^{-4}$ nA·Hz^{-1} is the external average synaptic coupling with the AMPA receptors.[15] The $+$ or $-$ sign refers to whether the motion direction is the preferred one or not the preferred one of the neural pool. In the schematic diagram Fig. 1, the neural population 1 is specifically selective for the leftward direction. If more dots move leftward, population 1 is favored and receives more stimulus. c' here is the motion coherence, which is used to indicate the degree of direction bias of moving dots. As shown in Fig. 1(b), when the motion coherence level is high, most dots move in the same direction. Figure 1(c) shows that dots move at a low coherence level. As seen, the dot motion hardly has an obvious directional bias. Note that μ_0 is the stimulus strength when there is no bias ($c' = 0\%$).

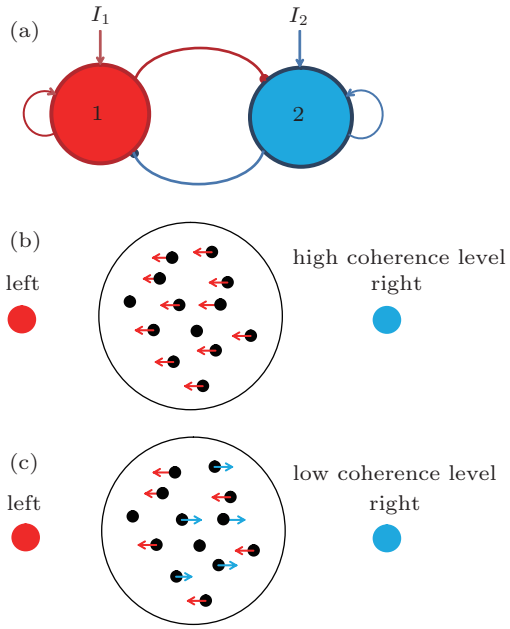


Fig. 1. (color online) (a) The schematic diagram of the reduced two-population decision-making model. This reduced model consists of two competing neural populations that are selective for leftward or rightward directions, respectively. The arrows represent excitatory connections, and the lines with solid circles represent inhibition. (b) and (c) The schematic representation of the random dots motion. For higher motion coherence, most dots move in one direction, whereas the dots move with no directional bias at a low motion coherence level.

In the original model,[15,16] the stimulus strength μ_0 is set to 30 Hz when the stimulus is presented. In this work, we discussed the system with different stimulus strength μ_0 and motion coherence c', and the detailed values are shown in the corresponding figure captions. We also found that the value of parameter b/a plays the role of input threshold in this dynamical neural model, which is represented by $\mathrm{Th_{in}}$ in this paper. We will call it the input threshold because the average activity of the selective neural population is very low when the corresponding stimulus input is below $\mathrm{Th_{in}}$. Once the input is beyond this threshold, the activity of the neural population increases significantly. Due to the great influences of parameters a and b on the dynamics of the decision-making model, we primarily discuss the corresponding details in the results and discussion section. The detailed values of parameters a and b are shown in the figure captions and text. The values of the rest of the parameters are set as shown above.

Here, we quantitatively uncovered such probabilistic landscapes from the underlying dynamics to explore the global properties of decision-making neural networks. The global stability of the neural circuits, which determines the difficulty of making decisions and changes of decisions can be explored by quantifying the probability landscape topography and the kinetics of state switchings. The population activity (firing rate) r_i of selective excitatory population i is a monotonically increasing function of the corresponding average gating variable S_i,[15,16] which means that a larger S_i indicates higher activities of neural population i. Therefore, quantifying the landscape of the network in the state plane of (S_1, S_2) is better for global understanding the dynamical process of decision making. Because we know the dynamical equations of the decision-making neural network, we can write the corresponding Langevin equations as: $\mathrm{d}I_{i,\mathrm{tot}}/\mathrm{d}t = \boldsymbol{F}(I_{1,\mathrm{tot}}, I_{2,\mathrm{tot}}) + \zeta$ through the transformation of coordinates ($\boldsymbol{S}$ to $\boldsymbol{I}$) because the noise term ζ is actually added to the driving force of the total current of neural population i. Then, we can obtain the potential landscape as the function of S_1 and S_2 with the method we discussed above through the transformation of coordinates ($\boldsymbol{I}$ to $\boldsymbol{S}$).

3. Results and discussion

3.1. Quantified attractor landscapes of the decision-making neural network

Although attractor landscapes have been introduced to describe the dynamics of decision-making neural networks, such landscapes still need to be further quantified. As we discussed in the method section, for a given dynamical neural system, we can obtain the temporal evolution of the probability distribution in the state space by solving the corresponding Fokker–Plank diffusion equation. Furthermore, we can quantify the potential landscape as $U = -\ln(P_{\mathrm{ss}}(\boldsymbol{s}))$,[20,21,23,32,34] where P_{ss} is the steady-state probability distribution. In the two-variable decision-making model, the dynamics of the system are determined by the external motion stimulus inputs to the two selective neural populations, which can be written as: $I_{\mathrm{motion},i} = J_{\mathrm{A,ext}}\mu_0(1 \pm c'/100\%)$, $i = 1$ and 2. Therefore, the absolute stimulus strengths μ_0 and the motion coherence c' (direction bias) are the key factors in decision-making tasks. In Fig. 2, we quantitatively mapped out the landscapes of the decision-making network in the state space plane of (S_1, S_2) for different stimuli strengths μ_0 ($\mu_0 = 0, 10, 30$ Hz, $c' = 0$ for the top row) and motion coherence levels ($c' = 0.2$, 0.3, 0.65, $\mu_0 = 30$ Hz for the bottom row).

Before stimulus onset (stimulus input strength $\mu_0 =$ 0 Hz), three stable attractors coexist in Fig. 2(a). As we have introduced in the model section, the average gating variables S_i at the steady state are positively correlated with the average firing rates of neural population 1, 2. Therefore, the gating variables S_i can reflect the mean activity of neural population. In the phase plane (S_1, S_2), the attractor that emerges at the bottom left corner corresponds to the undecided state with low activities of both neural populations, which is indicated by c in the landscape. One of the two decided states, a and b, on two sides emerges with higher activity of one neural population (group 1 or group 2, shown in Fig. 1(a)) and lower activity of the other one (group 2 or group 1). Decision making is the interplay between self-activation and mutual repression among

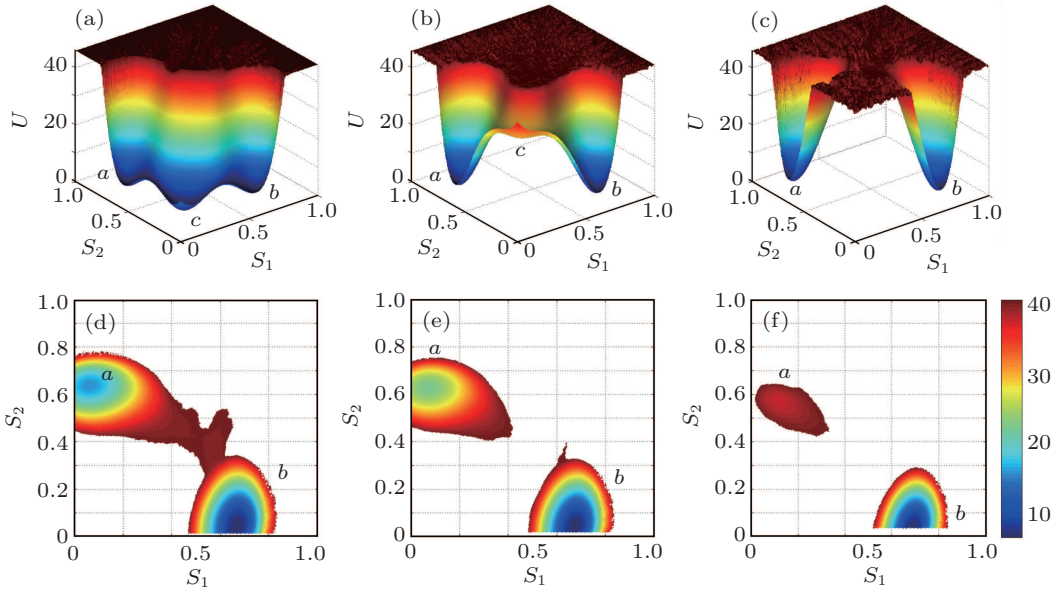


Fig. 2. (color online) The potential landscapes for different stimulus inputs and motion coherence. (a)–(c) Potential landscapes in the state space of average gating variables S_1 and S_2 at the zero coherence level for different stimulus inputs, where the stimuli strength $\mu_0 = 0, 10$ and 30 Hz, respectively. The central attractor corresponding to the undecided state is indicated by c in the figure, and a and b on two sides indicate the two decided states. (d)–(f) Two-dimensional potential landscapes at the non-zero coherence level, where $\mu_0 = 30$ Hz and the coherence $c' = 0.2$, 0.3 and 0.65, respectively. In all these subgraphs, the parameters $a = 269.5$ and $b = 108$ and the diffusion coefficient $D = 3.6 \times 10^{-7}$.

two populations. Without external motion stimulus inputs, the effective background input, I_0, can keep the decided states but cannot destroy the undecided state. For increasing stimulus strength ($\mu_0 = 10$ Hz) in Fig. 2(b), the central basin for the undecided state (c) becomes weaker. When the stimulus input is strong enough, the central undecided state c disappears, and only two decided states a and b remain on two sides (Fig. 2(c) where $\mu_0 = 30$ Hz). The undecided state is no longer stable, so the system driven by the attractor dynamics now can only stay in one of these two decided states. Therefore, a decision is made. Once the stimulus input is no longer presented to selective neural pools, the landscape returns to the one in Fig. 2(a). The decided states are still strong enough to hold the decision being made, which ensures the sufficient time to produce a motor response, such as a saccade to the target, before returning to the rest state.

The difficulty of this random-dot motion direction discrimination task varies depending on motion coherence c'. When coherence $c' = 0$, two selective neural groups receive the same stimulus. Coherence $c' = 1$ indicates that there is only one group receiving a stimulus. We can see in Figs. 2(d), 2(e), and 2(f) that once c' is not zero and the input strength $\mu_0 = 30$, the two basins of attraction are no longer symmetric. As the motion coherence c' increases, which indicates that one selective neural pool receives an increasing stimulus and the other one receives less, the basin of attraction at the upper left for the incorrect choice (indicated by a in the figure) becomes smaller and shallower. An advantage of our landscape theory is not only showing the positions of stable states but also giving the relative weight of each state. Accordingly, we can clearly see which state is more preferred. As shown in Fig. 2(f), the attractor for the incorrect choice at the upper left almost disappears when $c' = 0.65$. At zero coherence, the final decision is mostly determined by the fluctuations because of the symmetrical landscape. However, at a large coherence level, the effects of fluctuations on the decision are limited. When the motion coherence is large enough, the network is led to the correct choice in the beginning. This is because once the stimulus input is presented to drive the decision-making process, the system has been dominated by the attractor for the correct decision. It then requires strong fluctuations to overcome the barrier to reach the incorrect decided state a. Therefore, it is more likely to make a correct decision at larger coherence c'. Staying in a steeper basin of attraction initially for the case of higher c' also leads to the quick correct decisions. Once an incorrect decision is made because of fluctuations, it takes much more time to cross the barrier to reach the incorrect basin. Therefore, the average decision time is longer in error trails than in correct trails. These theoretical results are in agreement with the observations in decision-making experiments that show better performances and shorter decision times for larger coherence.[36,38] We will show more details in later sections.

3.2. Landscapes with varying stimulus inputs and decision paths on the decision-making landscapes

Figure 2 shows the landscapes of the decision-making neural network when the stimulus inputs are directly presented to the decision-making neurons. Some previous studies have suggested that changes of mind may occur after the initial decision because not all the information is used to make the initial choice.[39] Therefore, we would like to explore the situation in which stimulus input I_{motion} increases in time rather than the constant input (in time) presented directly during the decision-making process. When the varying input in time is taken into account, the underlying potential landscapes are more complicated and should be presented in the three-dimensional state space. First, we made an extreme assumption that the stimulus input changes relatively slowly compared with the dynamics of neural activities. This assumption is used only in Fig. 3(a). The varying input is described as $\mathrm{d}I_{\text{motion}}/\mathrm{d}t = \lambda I_{\text{motion}}$, and $\lambda = 0.0001$ is the varying rate of the stimulus input. Here, we use $I_{\text{tot},1}$ and $I_{\text{tot},2}$ (equivalent to S_1 and S_2 indicating the neural activities) as the horizontal axis, and the logarithmic function of input $\log_{10}(I_{\text{motion}})$ as the vertical axis. As shown in Fig. 3(a), before the input onset, there are three basins of attraction, and the central basin disappears gradually as the input increases.

The advantage of our approach over the previous studies[15,16] is that we not only quantify the relative weights of states on the landscape but also identify the optimal kinetic paths for the decision-making process. With a path integral approach,[22] we can quantify the weights of paths between each pair of states. The quantified optimal decision path has the highest probability between the undecided state and each of the two decided states. Furthermore, in our method, the way we quantify the decision path avoids time-consuming numerical calculations to obtain statistically meaningful data by averaging many trials in previous approaches. The details of the path integral approach are shown in the Appendices. As shown in Fig. 3, the pink lines indicate the optimal paths of decision making from undecided state c to decided states a and b. The system lies in the central basin of attraction at first. With fixed low inputs, the system can only get to the decided attractor on the two sides by going across the barrier. However, for changing inputs, the system is dominated by the central attractor at first. Then, it falls into the basin of one decided attractor as the input increases. The whole process is continuously dominated by attractor dynamics on the landscape in 3 dimensions (with two dimensions being the neural activities and one dimension being the stimulus input). Here we also show the paths from two decided states back to the undecided

state as a result of fluctuations, which are represented by red dotted lines. As a non-equilibrium system, the dynamics of the decision-making network are controlled by both the gradient force and the curl flux force. With the non-equilibrium flux force, we can see in the figure that the system does not return to the spontaneous undecided state following the same path of the decision-making process. The quantified paths show that the system still prefers to stay in the basins of attraction associated with the decided states even when there is no stimulus input presented. This landscape picture of the decision-making process in the brain resembles the Waddington landscape for differentiation and development.[20,40] The paths can quantify the detailed process of decision making in the brain, which will help us to understand the underlying mechanism of how the brain makes the decision. We also showed the potential landscape for the case of faster changing stimulus input in Fig. 3(b), where the varying rate $\lambda = 0.01$. We found that if the stimulus input increases faster, the probabilities of the two decided states corresponding to higher stimulus inputs are much larger (smaller potentials) than other states with a lower input. This result implies that the decision process is faster because the spontaneous undecided state disappears sooner.

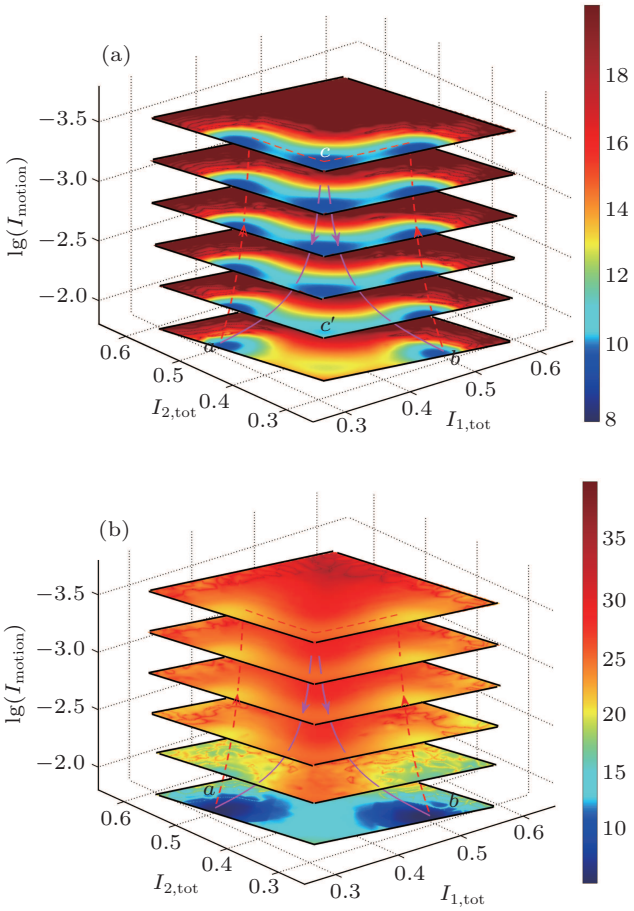


Fig. 3. (color online) (a) The potential landscape of the decision-making network with varying inputs and pathways. For the purpose of clear visualization, here we use $I_{1,\mathrm{tot}}$ and $I_{2,\mathrm{tot}}$ as x- and y-axis coordinates, which are equivalent to S_1 and S_2 for showing the positions of attractors. The pink lines indicate the paths of decision making from undecided state c to decided states a and b. The red dotted lines represent the paths from the two decided states back to the undecided state c. We should notice that once the external inputs are not presented, the system does not return to the rest state following the same path of the decision-making process. (b) The potential landscape of the decision-making network with faster varying input. The values of the parameters in Fig. 2 are $a = 270$, $b = 108$, $c' = 0$, and $D = 1.0 \times 10^{-6}$.

3.3. Landscape topography and the mean first passage time quantify the global stability and decision time of the decision-making system

Our quantified potential landscapes show the global properties of the neural network in the course of decision making. In previous studies,[15,16] the information on the positions of the attractors can be obtained. However, the quantitative information on the weight of each state of the multidimensional model and therefore the corresponding landscape were not known. An advantage of our landscape approach is that it provides a way to quantify the stability of the functional states though the quantification of their weights. The stability of attractors is very important for decision-making networks. For example, if the spontaneous state is not stable before the stimulus onset, more errors occur. If the decided state is not stable after the stimulus offset, the decision can be easily changed by small fluctuations. This also may result in that the decision cannot be held long enough to produce a timely response, i.e., a saccadic motor response in a visual motion direction discrimination task.

In this study we use the topography of the underlying landscape through the barrier height between basins of attraction to quantify the stability of stable states. Here, the barrier height is defined as $U_{\mathrm{saddle}} - U_{\mathrm{min}}$, U_{min} is the potential minimum of one local stable state and U_{saddle} is the potential at the saddle point between two stable states. In addition to barrier heights, we also quantified the mean first passage time (MFPT) from one stable state to another to describe the stability of stable attractor states (see Appendixes for methods to acquire the MFPT). It turns out that the mean first passage time is closely related to the barrier height. It will take a longer time to escape the attractor with a higher barrier.

First, we showed the landscapes at different fluctuation levels before the stimulus inputs onset in Figs. 4(a) and 4(b) through changing diffusion coefficient D, which measures the strength of fluctuations. We can see for a larger diffusion coefficient, the potential barriers between attractors are lower, which means that such attractors are less stable. Figure 4(c) shows the details of how the barrier height decreases as the fluctuations, characterized by diffusion constant D, increase. This result is consistent with the above discussion that the basins of attraction are shallower for larger fluctuations. Then, we calculated the corresponding MFPT both from decided state a (lying on the left) to saddle point s and central undecided state c to s. We can see from Fig. 4(d) that escaping the

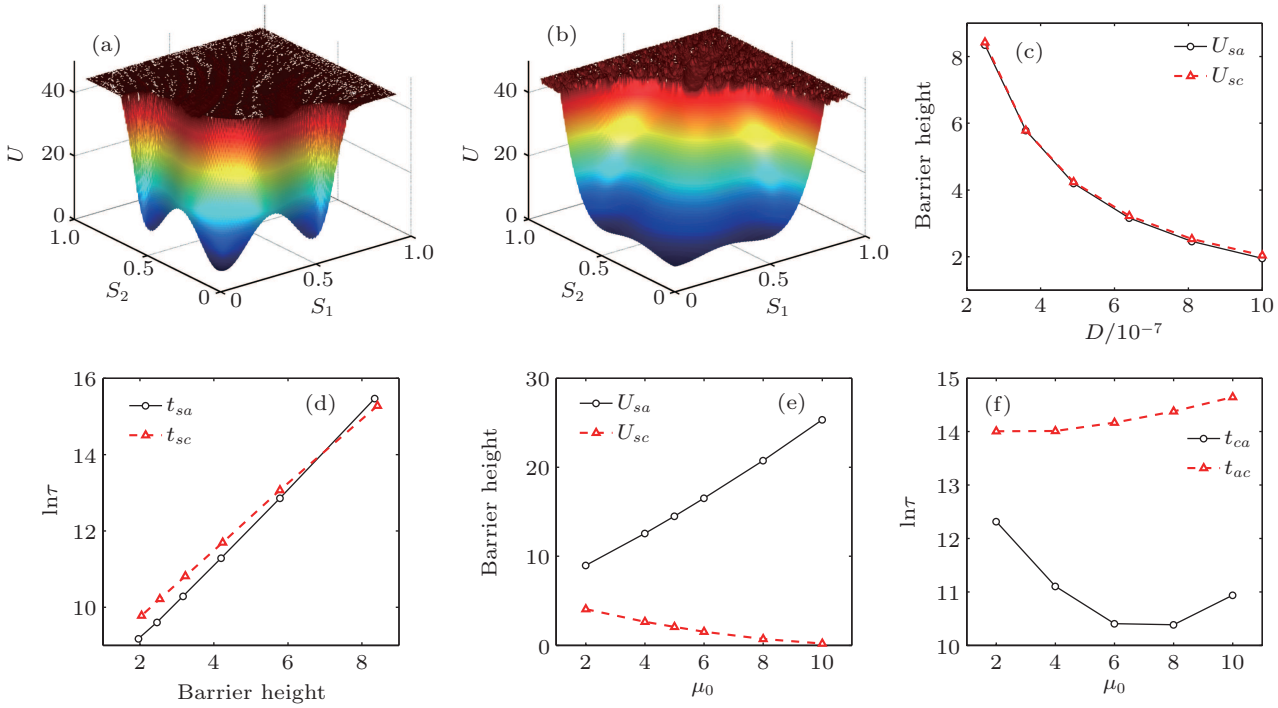


Fig. 4. (color online) (a), (b) Potential landscapes for different diffusion coefficients, where $\mu_0 = 0$ Hz, $c' = 0$, and the diffusion coefficient $D = 1.6 \times 10^{-7}$, 1.0×10^{-6}, respectively. a and c represent the decided state and undecided state, respectively. s represents the saddle point between a and c. (c) The barrier heights versus D. Here $U_{sa} = U_s - U_a$ and $U_{sc} = U_s - U_c$. (d) The barrier heights versus the corresponding mean first passage time. τ_{as} and τ_{cs} indicate the mean first passage time from state a and state c to saddle point s, respectively. (e) The barrier heights versus input strength μ_0. (f) The mean first passage time versus input strength μ_0. τ_{ca} indicates the mean first passage time from state c to state a. τ_{ac} indicates the mean first passage time from state a to state c. In all these subgraphs, parameters $a = 269.5$ and $b = 108$ and motion coherence $c' = 0$.

basin of attraction with a higher barrier takes longer. A longer (shorter) escape time implies less (more) ability to move to other places in the whole system and therefore more (less) stable. The escape time quantifies the global stability of the system. Therefore, the landscape topography through the barrier height can quantitatively measure the global stability of attractors, in addition to the escape time.

The central undecided attractor disappears very quickly when the stimulus input strength increases. Therefore, to quantify the stability of different function states, we show here the barrier heights and the corresponding MFPT versus the varying input for a short range, in which the stimulus strength μ_0 varies from 0 to 10 Hz. As shown in Figs. 4(e) and 4(f), the central attractor that represents the undecided state becomes shallower (smaller U_{sc}), and the attractors of two decided states become deeper (larger U_{sa}) for a larger input. Furthermore, the corresponding MFPT also shows that it is easier to escape the undecided attractor as the stimulus input increases. On the contrary, the decided attractors become deeper and more stable due to the increase of the corresponding MFPT for escape. The solid line in Fig. 4(f) shows nonmonotonic behavior. This illustrates that the barrier height cannot always be used as the quantitative measurement for global stability, but the MFPT can.

The time taken in the process of decision making is always an issue of concern. Another benefit of quantifying the mean first passage time is that we can quantitatively explore the decision-making speed or time (from the undecided state to a decided state) under different biological conditions. As shown in previous research, when the motion coherence increases (the decision task becomes easier), the decision time to make the correct choice decreases monotonously and the decision time in error trials is always longer.[15,36,38] Here, we obtain similar results by solving the corresponding MFPT. As shown in Fig. 5, we can see that for a lower motion coherence level, the decision times in the correct and incorrect trials are nearly the same. This is because the two populations of decision-making neurons have similar inputs, and it is difficult to make a choice. As the coherence level increases, the decision time in the correct trial decreases monotonously, and it increases in the incorrect trial. The decision time in the error trial is always longer. Our theoretical predictions are in good agreement with the experimental results. The difference is that when the coherence is large enough, errors may not happen in the experiments. In our probabilistic landscape description, we used the mean first-passage time to quantify the decision time. Theoretically, we could obtain the decision time for any conditions by solving the equation. We found when the coherence is large enough, the time required to make the wrong decision is so long that it may not happen in practice.

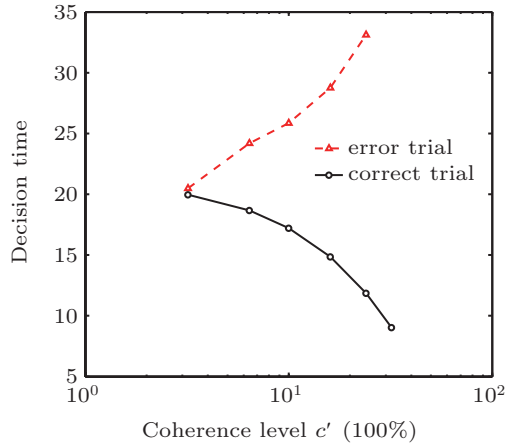


Fig. 5. (color online) The decision time in the correct and error trials. Here the parameters are $a = 269.5$, $b = 108$, $\mu_0 = 30$ Hz, and $D = 3.6 \times 10^{-7}$.

3.4. Quantifying the mechanisms of the speed-accuracy tradeoff of decision-making from the landscape perspective

When people make decisions, they often face opposite demands in speed and accuracy. How this speed-accuracy tradeoff (SAT) is implemented in neural decision-making circuits has received attention in recent years.[41–43] In previous models of the decision-making network, the activities of decision-making neurons increase gradually as the stimulus input is presented. Once the activities reach the decision threshold, the decision is made. The decision-making neurons can be seen as integrators of stimulus input information. Mathematically speaking, an increase in the initial activities of integrator neurons (baseline) and the reduction of the decision threshold seem to be equivalent for speed emphasis because both ways shorten the process of information accumulation. Meanwhile, decisions are less accurate because the decision-making process can be more easily affected by the fluctuations due to the shortening distance between the baseline and the decision threshold. Many modeling studies have implied a lower decision threshold as the mechanism for speed emphasis.[44,45] However, recent human brain-imaging studies and neurophysiological recordings provide strong evidence for the changing-baseline hypotheses.[43,46,47] The corresponding intrinsic mechanisms of the speed-accuracy tradeoff in the attractor model need to be quantified. The advantage of quantifying the potential landscape is that it can directly and quantitatively reflect the influences of varying parameters with specifically biological meanings on the landscape, which can help us to uncover the mechanisms of the decision-making process.

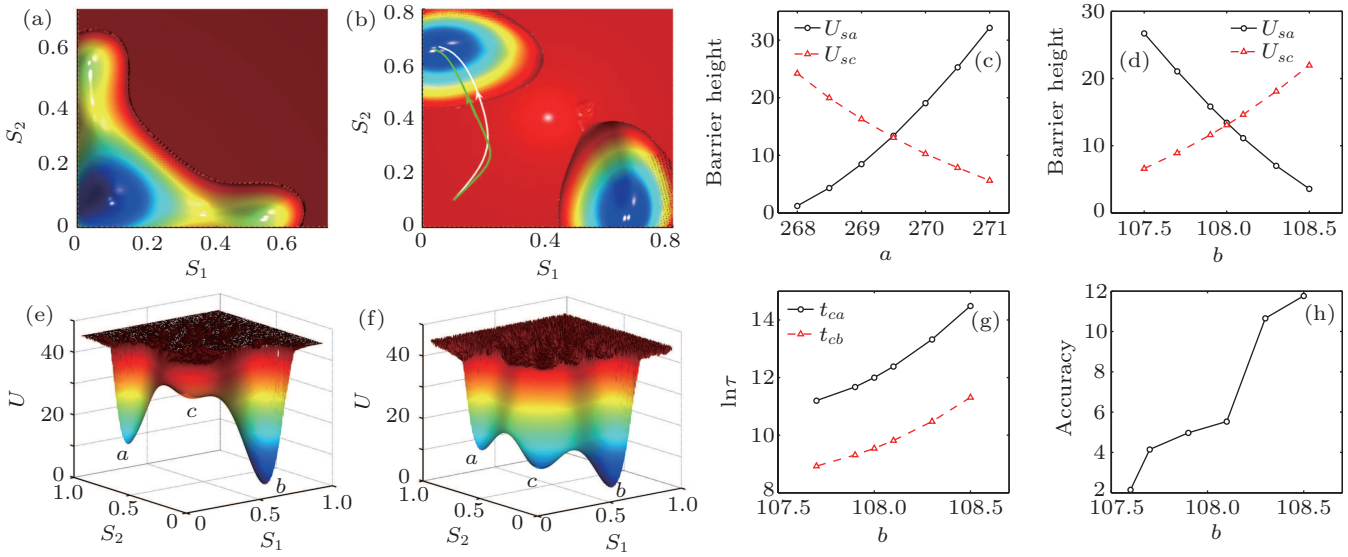


Fig. 6. (color online) (a) The two-dimensional potential landscape for a higher input threshold before the stimulus inputs presented ($\mu_0 = 0$ Hz). (b) The two-dimensional potential and pathways for constant stimulus input $\mu_0 = 30$ Hz and different parameter b. The green line and white line show the decision-making pathways with different input threshold b/a where $b = 108.5$ and 107.5, respectively. In subgraphs (a) and (b), parameters $a = 269.5$ and $b = 108$ and the diffusion coefficient $D = 3.6 \times 10^{-7}$. (c), (d) The barrier heights versus parameters a and b, respectively. Here $\mu_0 = 0$ Hz, $c' = 0$, and the diffusion coefficient $D = 1.6 \times 10^{-7}$. (e), (f) The potential landscapes for different input thresholds when a biased input is presented, where the parameter $b = 107.5$ and 108.5, respectively. Attractors a and b represent the incorrect choice state and correct choice state, respectively. c represents the undecided state. (g) The first passage time versus parameter b. (h) The ratio of the probability of the path of the correct choice to the error one versus parameter b. In subgraphs (e) and (h), parameters $\mu_0 = 5$ Hz, $c' = 0.24$, $D = 1.6 \times 10^{-7}$, and $a = 269.5$.

Based on the changing-baseline hypothesis, theories are proposed to explain how the speed-accuracy tradeoff is controlled in the cortical-basal ganglia circuit.[43] The cortical theory suggests that cortical decision-making integrator neurons receive additional excitatory input (the baseline is increased) with speed emphasis. Previous theoretical studies support this theory with the one-dimensional non-linear diffusion model.[11] In our attractor landscape, presenting additional inputs to selective decision-making integrator neurons can be described as the decision process initiated at state c' instead of state c in Fig. 3(a) because the initial activities of the neurons (baseline) are increased. The central attractor for

undecided state c' is not as strong as c, and it is closer to decided state a or b, which makes the decision faster. Although information accumulation will take a shorter time to exceed the threshold, it is more likely to be influenced by the noises to make wrong choices.

Differently from the cortical theory, the striatal theory suggests that with speed emphasis, the striatum receives excitatory input from cortical (non-integrator) neurons, increasing striatal activity and thus decreasing the inhibitory control of the basal ganglia over the brain.[43] Because of the strong functional projections from the basal ganglia back to the cortex via the thalamus, the striatal theory also predicts that the baseline of the cortical decision-making integrator neurons is increased with speed emphasis. As a result, the decisions are fast but error-prone. How can this mechanism be quantitatively explored with our landscape approach? To address this issue, we focused on the input–output function of the selective integrator neurons in the mathematical model. As we introduced in the model section, we defined $\mathrm{Th_{in}} = b/a$ as the input threshold of the decision-making neural network model. We found the activities of decision-making integrator neurons are very low when the corresponding stimulus input is below $\mathrm{Th_{in}}$. Once the input is beyond this threshold, the activity of the neural population increases quickly.

Lower input threshold $\mathrm{Th_{in}}$ indicates that the selective neurons can be more effectively activated by the same stimulus inputs. In other words, the stimulus inputs become more effective. Therefore, the effects of decreasing input threshold $\mathrm{Th_{in}}$ here are equivalent to less inhibitory control in the decision-making integrator neurons, which is consistent with what the striatal theory suggests. According to the input–output function of integrator neurons, a lower $\mathrm{Th_{in}}$ increases the baseline. In Fig. 6(a), we can clearly see that before the stimulus inputs are presented, the central basin for the undecided state becomes deeper and larger when $\mathrm{Th_{in}}$ is higher (larger parameter b), compared with the landscape shown in Fig. 2(a) where the central attractor is approximately as stable as the other two basins for decided states. We also show the decision paths for different input threshold $\mathrm{Th_{in}}$ in Fig. 6(b). When $\mathrm{Th_{in}}$ is higher, the path indicated by the green line prefers to stay in the states where the activity difference between two competing neural groups is smaller (along the diagonal of the square state plane). In other words, the decision is more difficult to make. Then, we plotted how barrier heights of U_{sa} and U_{sc} change with the parameters a and b, respectively in Figs. 6(c) and 6(d). We can see the potential barrier from central undecided state c to decided state a (U_{sc}) increases as $\mathrm{Th_{in}}$ increases, and on the contrary, the barrier from decided state a to central undecided state c (U_{sa}) decreases. This indicates a larger $\mathrm{Th_{in}}$ results in stronger and more stable central basin of attraction for the undecided state. This result can be easily understood. For a larger input threshold, it requires stronger stimulus input to excite the decision-making neurons to reach the decided attractors.

Furthermore, we quantitatively explored how the input threshold affects the performance and decision time of the decision-making processes with the landscape approach. In Figs. 6(e) and 6(f), we show the potential landscapes for two different input thresholds $\mathrm{Th_{in}}$ when a biased input is presented ($c' = 0.24, \mu_0 = 5$ Hz). Figures 6(e) and 6(f) show the central undecided basin is more stable, and both barriers to two decided basins are higher for a larger $\mathrm{Th_{in}}$. Then, we show the details of how the decision time increases as the input threshold $\mathrm{Th_{in}}$ increases in Fig. 6(g) by increasing parameter b. As we have discussed above, it is easier to make a decision for an unstable central basin because of its shorter decision (escaping to the decided state) times. In the random dot motion tasks, shorter decision times are always accompanied by more errors. Here we studied the performance of the neural network with a path integral method.[22] The advantage of the path integral method is that it can quantify the weights of the optimal path between each pair of states. The basin for the correct choice state is indicated by b in Figs. 6(e) and 6(f). Once the system has reached state b from spontaneous undecided state c, such a trial is regarded as a correct one. Otherwise, an error choice emerges if the system reaches the wrong decided state indicated by a. Here, we defined the performance (accuracy) of the decision-making task as the ratio of the weight of the optimal correct path (P_{cb}) to the weight of the error one (P_{ca}). We can see in Fig. 6(h) that ratios P_{cb}/P_{ca} are all larger than 1, which implies that the probability of making a correct choice is always larger than that of an error one. Figure 6(h) also shows the performance is worse when parameter b is smaller (lower $\mathrm{Th_{in}}$). Therefore, we found that with a lower $\mathrm{Th_{in}}$, the baseline is increased, and the decision speed is improved at the expense of reducing accuracy. These theoretical predictions are consistent with the speed-accuracy tradeoff observed in experiments.[47–49] Our predictions can be tested in future experiments to distinguish which mechanism is more important in the speed-accuracy tradeoff control. The cortical theory wins if the cortical neurons receive the additional input. The striatal theory better explains if there are additional inputs to the striatum.

3.5. Energy cost and the speed–accuracy–energy tradeoff of decision making

In addition to speed and accuracy, the energy cost is another focus of attention in the decision-making process. Both receiving additional excitatory input and lowering input threshold $\mathrm{Th_{in}}$ increase the baseline and play similar roles in the speed–accuracy tradeoff with speed emphasis. However, whether two mechanisms show similar natures when the en-

ergy cost is taken into consideration remains to be addressed. It is expected that speed emphasis may cost more energy with faster speed from intuition. To test this prediction, we calculated the entropy production rate as a measurement of energy dissipation per unit time[28] (see details in Appendixes). We found the total entropy production rate (the change in the entropy inside the system adds to the entropy flow rate from the environments) is always larger or equal to zero. It has the physical meaning of the energy cost or dissipation rate (the temperature is regarded as a constant for simplicity). For a given non-equilibrium dynamical system (all parameters are set), there will always be a certain amount of energy dissipated in unit time (measured by the entropy production). The entropy production rate is closely related to the probability flux. The flux is the origin of the entropy production. Therefore, quantifying the flux of the decision-making network provides us with a chance to explore the energy cost in the decision-making processes.

Figures 7(a) and 8(a) show that the entropy production rate (EPR) is larger with lowering input threshold represented by the smaller parameter b and the increasing additional input, indicated by the larger input strength μ_0. Our results suggest that more energy is dissipated in unit time with speed emphasis. Neuroimaging techniques such as positron emission tomography (PET) and fMRI are used to measure neuronal activities. We should notice that the nature of these brain-imaging methods is not detecting brain activity directly but rather measuring signals that reflect brain energy consumption.[50] In fact, PET records change in blood flow and oxygen consumption, whereas fMRI signals reflect the degree of blood oxygenation. We know that the brain energy cost comes from the oxidation of glucose delivered in the blood. Although we cannot precisely measure the energy cost in the brain, these neuroimaging recordings can give us some information about the trend in energy consumption through oxygen. Previous fMRI studies show that in easier decision tasks the blood-oxygenation-level-dependent (BOLD) signal increases greatly in the sensory processing area.[51,52] With lower difficulty levels, the activities of decision-making neurons increase quickly, just as the decision-making process with speed emphasis can. Our predictions are consistent with the fMRI studies. Furthermore, we explored the total energy cost in decision makings for two modulating mechanisms. Here, we calculated the total energy cost as the entropy production rate multiplied by the decision time. To make the discussions clearer and more complete, we also show how the decision time changes as the parameter b and input strength μ_0 vary in Figs. 7(a) and 8(a).

Let us focus now on the speed–accuracy tradeoff mechanism by varying input threshold $\mathrm{Th_{in}}$, as the striatal theory suggests. As shown in Fig. 7(b), the total energy cost in decision making increases when the input threshold increases (larger parameter b). Although the energy cost in unit time

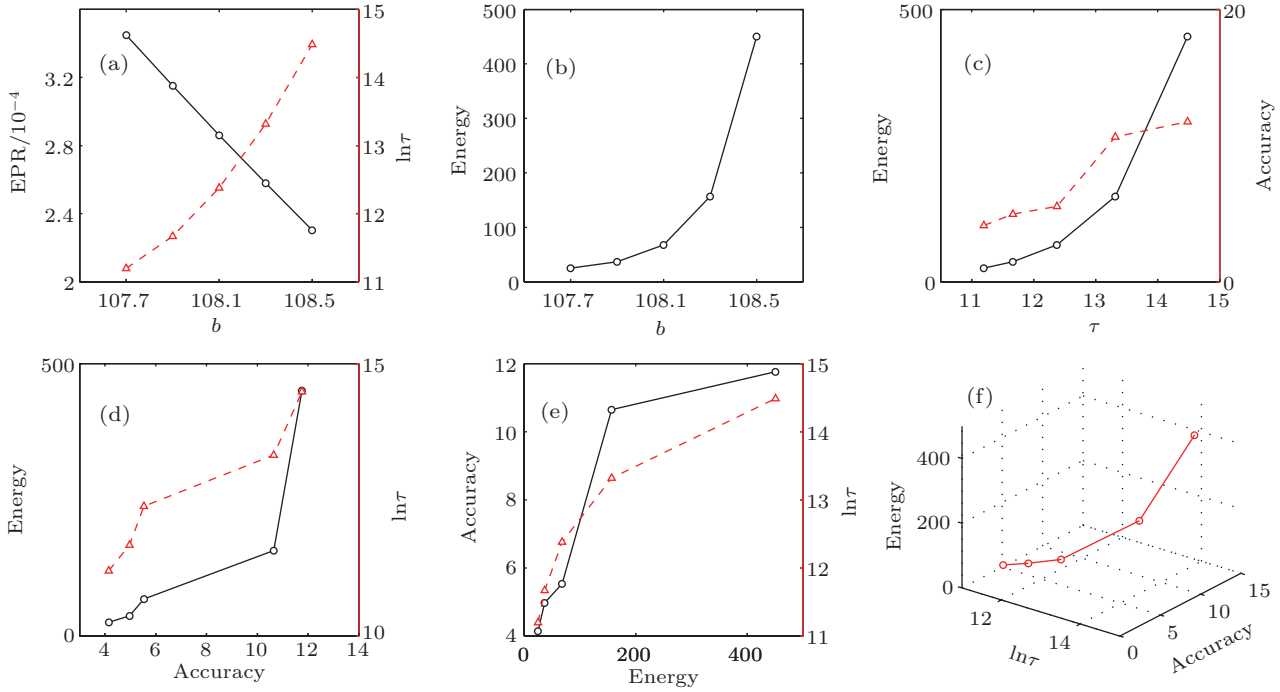


Fig. 7. (color online) (a) The entropy production rate (EPR) versus parameter b. The decision time represented by the MFPT versus parameter b shown with the red line. (b) The total energy cost versus parameter b. (c) With speed emphasis, less energy is required, but the performance is worse. Here the accuracy is represented by the ratio of the probability of the path of the correct choice to the error one. (d)–(f) The inter-relationship among the speed, accuracy, and energy cost based on the varying input threshold. In all subgraphs, parameters $a = 269.5$, $\mu_0 = 10$ Hz, $c' = 0.24$, and $D = 1.6 \times 10^{-7}$.

is lower for a higher input threshold, the total energy cost is larger because of the significant increase in the decision time. In Figs. 7(c)–7(f), we show the inter-relationship among speed, accuracy, and the energy cost with varying input threshold. Here, the accuracy is represented by the ratio of the probability of the path of the correct choice to the error one ($P_{\text{correct}}/P_{\text{wrong}}$). When the speed is the main concern of the decision making, with speed emphasis (Fig. 7(c)), the performance of the decision making is worse, but it costs less energy. If the accuracy is the main concern in decision making, the decision accuracy is demanded (Fig. 7(d)), and a longer decision time and higher energy costs are required. When the energy cost is the main concern in decision making (a lower energy cost) (Fig. 7(e)), the decision can be made faster, but the accuracy is worse. Figure 7(f) shows the full interrelationship among speed, accuracy, and the energy cost in decision making with varying input thresholds.

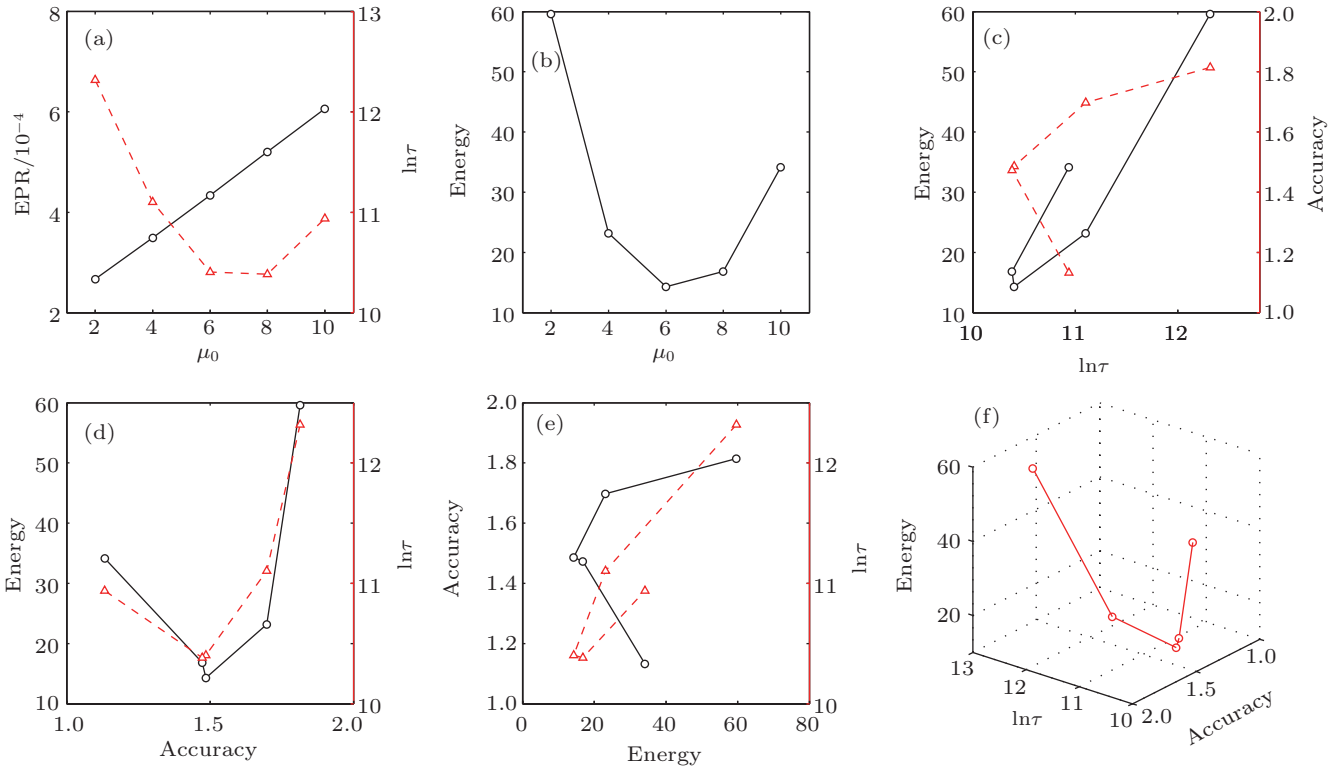


Fig. 8. (color online) (a) The entropy production rate (EPR) versus motion input strength μ_0. The decision time represented by the MFPT versus input strength μ_0 is shown with the red line. (b) The total energy cost versus motion input strength μ_0. (c) The total energy cost increases as the decision time increases. For fast (slow) decisions, the performance can be improved with decreasing (increasing) decision time. Here the accuracy is represented by the ratio of the probability of the path of the correct choice to that of the error one. (d)–(f) The inter-relationship among the speed, accuracy, and energy cost based on presenting additional input to cortical integrators. In all subgraphs, parameters $a = 269.5$, $b = 108$, $c' = 0.24$, and $D = 3.6 \times 10^{-7}$.

In addition, focusing on the speed–accuracy tradeoff mechanism proposed in the cortical theory, we find that the energy cost does not change monotonously when the cortical decision-making integrator neurons receive larger additional input. As shown in Fig. 8(a), the decision time decreases quickly at first and then decreases more smoothly. The slight increase in the decision time next can be understood as the fact that when $\mu_0 = 10$, the central attractor of the undecided state disappears and the system is more easily influenced by the fluctuations and noises to go to the wrong attractor first, which results in a slightly longer decision time. By contrast, the entropy production rate increases monotonously. Therefore, the total energy cost shows the non-monotonic nature with an increasing additional input. The inter-relationship among speed, accuracy, and the energy cost with a varying additional input is shown in Figs. 8(c)–8(f). If the speed is the main concern of the decision making, there is an optimal (minimal) decision speed (Fig. 8(c)) with a nearly optimal (minimal) energy cost and reasonable accuracy performance. A higher accuracy still requires a longer decision time (slower decision speed). We now discuss the situation when the accuracy and performance are the major concern of decision-making (Fig. 8(d)). We can see in Fig. 8(d) that reasonable but suboptimal accuracy and performance can be achieved with optimal energy cost and speed. With the best accuracy and performance, the energy cost and time for decision making are higher than the optimum. If the energy cost is the main concern for decision making (Fig. 8(e)), the decision accuracy and performance may

not be the best with the least energy cost; however, we can still reach a faster speed based on the varying additional input mechanism. Figure 8(f) shows the entire interrelationship among speed, accuracy, and energy cost in decision making with varying additional input to cortical integrators.

In summary, we have quantitatively discussed the cortical theory and the striatal theory of the speed–accuracy tradeoff in decision making. If the energy cost is taken into consideration, there should be a speed–accuracy–energy tradeoff. With speed emphasis, although the accuracy is sacrificed, the energy cost may be minimized. Our results imply there is an optimal balance among speed, accuracy, and the energy cost with a varying additional input. They may also serve as a basis for the optimal design of decision-making with speed, accuracy, and energy cost. The fMRI study supports our predictions that more energy costs in unit time with speed emphasis, but the total energy cost in the whole decision process still needs to be confirmed in future experiments.

3.6. Changes of mind in decision making

In our daily lives, making decisions is often accompanied by situations in which we change our minds. Usually, such changes can lead to the correction of initial errors. An additional strong opposite stimulus may result in decision reversal because the corresponding attractor landscape reverses. However, a decision reversal sometimes happens without adding an input with an opposite direction. Here, the changes of mind we discussed refer to making different choices under no changes in the direction of the stimulus inputs (random dots motion coherence c') after an initial decision has been made.

Without an opposite input, the two attractors of the decided states do not reverse. We obtain some insights from the recent research findings: when strong inputs are presented to both selective decision-making neural populations, a new state emerges.[15,44] From Fig. 9(a), where stimulus strength $\mu_0 = 50$ Hz and motion coherence $c' = 0$, we can see there are only two distinct basins of attraction each representing two decided states. As the input increases, a new attractor emerges in the center with high activities on both populations in Fig. 9(b) ($\mu_0 = 60$ Hz). Here, we use larger strength of stimulus μ_0 instead of adding a common input to both neural pools for simplicity, and this does not affect the results. The new stable state indicated by d in Fig. 8 corresponds to the state where both decision-making neural groups have higher activities or firing rates. Therefore we can call this state a "double-up" state, compared to the two decided states a and b with only one neural group activated ("single up"). This "double-up" state d becomes increasingly stronger as the input increases. In Fig. 9(c) ($\mu_0 = 65$ Hz), the system is completely dominated by this "double-up" state. Therefore, we can understand the whole process of changes of mind from the potential landscape perspective. Once a decision has been made, the system stays at one of the decided states (a or b). Then, a higher common input is presented to both selective neural populations, which leads to the domination of one activated central basin (d). However, this new attractor will disappear soon after the inputs return to normal levels (the landscape returns to the one with only two decided states). Therefore, the network has to make a new choice after being attracted to this new central basin of attraction, as shown in Fig. 9(c). If the system makes a different choice with the help of biased inputs and fluctuations, a change of mind occurs. Our results are supported by spiking model simulation studies, which showed that with larger stimulus inputs the firing rates of both decision-making neural populations stay at a high level ("double-up") during changes of mind rather than only one neural group being highly activated according to winner-take-all.[44] These findings suggest that changes of mind are due to the emergence of the new central basin of attraction, or a new "double-up" state, with high activities in both populations. In fact, this "double-up" state has been found in the previous experiments before the random dot motion onset.[35,37] It is explained as the decision-making integrator neurons receiving a target input during the target presentation.[16,44] However, the role of this state in the process of an initial decision is still unclear. Now because the "double-up" state is so important in changes of mind, where does the additional input come from after the initial decision has been made? It is suggested that not all the information is used to make the initial choice. The changes of mind may be caused by the unprocessed information that is not presented before the first decision.[39]

Figures 9(d)–9(f) show that the landscapes when large inputs (here $\mu_0 = 55$ Hz) are presented at non-zero coherence levels, $c' = 0.02$, 0.06, and 0.12, respectively. We can see that, for biased inputs, attractor b for the correct choice is more attractive. The stability of attractor b guarantees that changes in the initial correct decisions are not likely to occur. On the contrary, if the network made a wrong decision at first, changes may happen more easily. The reason is that although the network has a second chance to make a decision due to the very large stimulus input, it is still more likely to be attracted to the stronger basin of attraction for the correct choice after the large input offset. Therefore, there are more chances for changes to the correct choice.

According to our potential landscape theory, we can provide a physical explanation of other experimental findings in changes of mind. Previous works show that with increasing coherence, the probability of changes to the wrong choice from the correct one decrease monotonically.[39,44,45] In the meantime, changes to the correct choice peak at intermediate motion strength and then decrease gradually. First, we need to sum up the whole process of changes of mind in three nec-

essary steps: making the initial choice, then being attracted to the new basin of attraction or, in other words, getting to a "double-up" state (high activities for both groups of neurons, the central basin) and, at last, making a different choice. A change of mind requires that process. Then these experimental findings can be easily understood with our potential landscape theory.

Although changes from the wrong to the correct choice are always more frequent than changes from the correct to the wrong choice, the trends of the probabilities of the two types of changes versus the motion coherence are slightly different. We have shown that the network is more likely to make a correct decision at a higher coherence level. Compared with the landscape shown in Fig. 9(b) whose stimulus strength $\mu_0 = 60$, we can see that for the cases of biased inputs shown in Fig. 9(f) where the coherence is $c' = 0.12$, even the input becomes large, and the basin for correct choice state b is still very strong and stable. Such a large input is still not strong enough to force the system to escape from the attractor for the correct choice. We also found that new central attractor d cannot emerge when the motion coherence is too large, which implies that the attractor with the correct decision is the only dominated one. Therefore, for the case that most initial choices are correct at high coherence levels, changes may not happen. Furthermore, even though a second choice occurs, it is still not possible to make errors. In other words, mind changes do not occur due to the biased potential landscape. This is why the overall trend of the probability of changes is decreasing gradually with increasing coherence. However, at low coherence levels where c' is smaller than 0.1, the potential landscape is almost symmetric, and there are more initial errors. We also noticed that at such low coherence levels, it is increasingly likely to go to the central double-up state from the wrong decision attractor as the coherence increases, and larger coherence results in a higher probability of changes to the correct choice. On the contrary, with increasing coherence the initial correct choice is more likely to be kept, as we have discussed. Therefore, at low motion coherence levels, it is more likely for the neural system in the brain to make a different decision and the changes to the correct decision may even increase with increasing coherence.

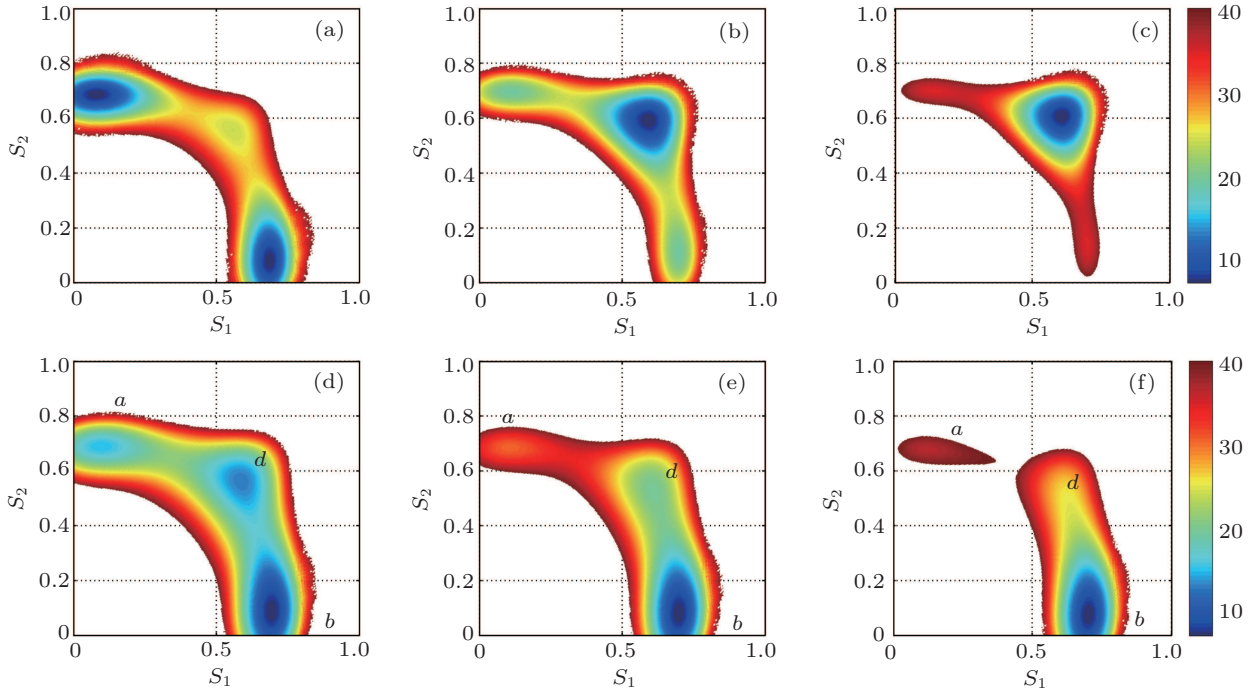


Fig. 9. (color online) Comparison of potential landscapes with different large inputs. (a)–(c) The two-dimensional potential landscapes for different large inputs at zero coherence level. The strength of stimulus $\mu_0 = 50$, 60, and 65 Hz respectively. (d)–(f) The two-dimensional potential landscapes for large input ($\mu_0 = 55$) when coherence $c' = 0.02$, 0.06, and 0.12, respectively. In all subgraphs, parameters $a = 269.5$, $b = 108$, and $D = 3.6 \times 10^{-7}$.

We also used a path integral method to quantify the weights of the paths of changes of mind to give a quantitative explanation of the experimental observations in changes of mind.[22] We can compare the probabilities of two paths in changes of mind for certain coherence c'. In Fig. 10(a), we use P_{right} to indicate the probability of the optimal path that the decision network made a wrong choice at first and then changed from the wrong to the right choice. P_{right} here is quantified by $P_{ca} \times P_{ad} \times P_{db}$. Contrarily, the $P_{\text{wrong}}(P_{cb} \times P_{bd} \times P_{da})$ represents the probability of the optimal path from the right to

the wrong choice. Our theoretical results with the path integral approach are consistent with the experimental observations, which are shown in Fig. 10(a). We can see that the ratio $P_{\rm right}/P_{\rm wrong}$, is always larger than 1, which indicates that the probability of changing to the correct choice is always larger than changing to the wrong choice. $P_{\rm right}/P_{\rm wrong}$ increases first and then falls down to 1 as coherence c' increases from 0 to 1. This result is consistent with the experimental results and our qualitative explanation discussed above. With unbiased inputs ($c' = 0$), the probabilities of changes to the right choice and changes to the wrong choice are the same. At low coherence levels, changes to the right choice are relatively more likely to happen than changes to the wrong choice. When the coherence c' is close to 1, neither of the two changes may happen, and $P_{\rm right}/P_{\rm wrong}$ drops to 1 again.

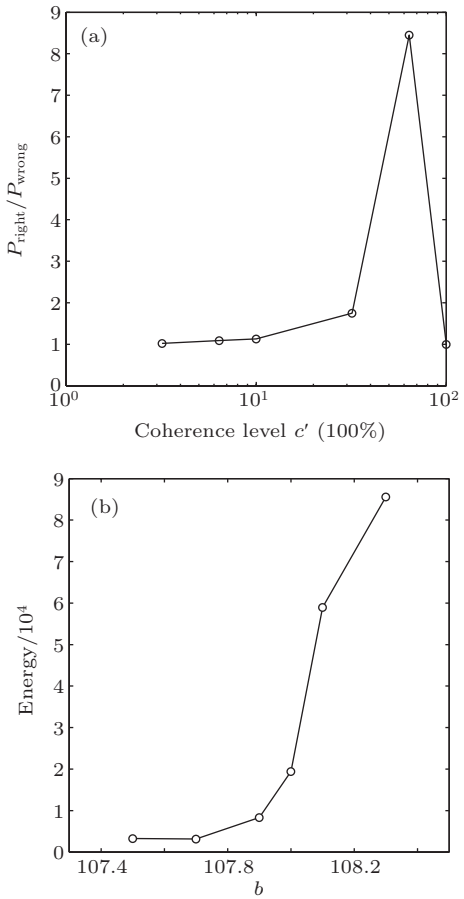


Fig. 10. The ratio of the probability of two paths and the energy cost of changes of mind. (a) $P_{\rm right}$ represents the probability of the optimal path that the decision network made a wrong choice at first and then changes from the wrong to the right choice. Contrarily, $P_{\rm wrong}$ represents the probability of the optimal path from the right to the wrong choice. (b) The total energy cost in changes of mind versus parameter b.

We believe the change of mind is an intrinsic mechanism of improving performance in decision-making tasks. Initial correct decisions are more likely to be kept. For error trials, changes of mind give the neural network a second chance to make a new choice; thus, many errors will be corrected. We know that a longer reaction time is important for the performance (accuracy) of decision making. There is also evidence showing that when subjects were asked to perform decision tasks more slowly, there were fewer changes of mind and more accurate initial decisions.[39] We have discussed the mechanism of the speed–accuracy tradeoff in decision making from the landscape perspective. Here, we also explored the effects of input threshold $\rm Th_{in}$ on the potential landscapes during the process of changes of mind. In Fig. 11, as the threshold $\rm Th_{in}$ decreases (smaller parameter b), which indicates that the stimulus inputs are more effective to activate the decision-making neural pools, we can see the new central attractor ("double-up" state d) that is crucial for changes of mind becomes stronger. The stronger new central attractor implies that the probability of making a second choice is higher, particularly for initial errors, with increasing inputs. Comparing the relative weights of the three attractors shown in Figs. 11(d), 11(e), and 11(f), we also find that the new central attractor is always stronger than the attractor with the incorrect decision for a lower input threshold, whereas the strength of the correct attractor changes little. This finding suggests that changes to the correct choice are more likely to occur, and the initial correct choice is still likely to be kept. Behavioral data in the experiments of previous studies[39] show there are more changes with a shorter decision time, and our theoretical results suggest most of these incremental changes will correct initial errors.

Lower input threshold $\rm Th_{in}$ reduces the difficulty in making a choice, both correct and incorrect. It also makes the new central attractor ("double-up" state) stronger for more changes. Therefore, we can conclude although the time pressure may lead to more initial errors, there will be more changes made to correct these errors if there are large enough inputs presented. The speed–accuracy tradeoff always works. Fortunately, the mechanism of changes of mind guarantees the reasonable performance of decision making with speed emphasis as long as people have the chance to make the changes. We have discussed the speed–accuracy–energy tradeoff. It seems that not focusing on accuracy may save energy. The conclusion is not clear if we take changes of mind into consideration. A faster speed may result in more initial errors. Once the initial error is corrected by changes of mind, an additional energy cost is required. As shown in Fig. 10(b), much more energy is required for changes of mind than for the initial choices, particularly for a larger input threshold. On the contrary, with enough time, the initial decisions are more accurate; therefore, there is less need to make changes and a lower additional energy cost. With accuracy emphasis, one has to choose between a higher energy cost in the initial decision and additional energy cost in changes of mind. Regardless, more energy is required for better performance in decision making. Our theoretical predictions provide guidelines for future experiments on the speed–accuracy–energy tradeoff in decision making.

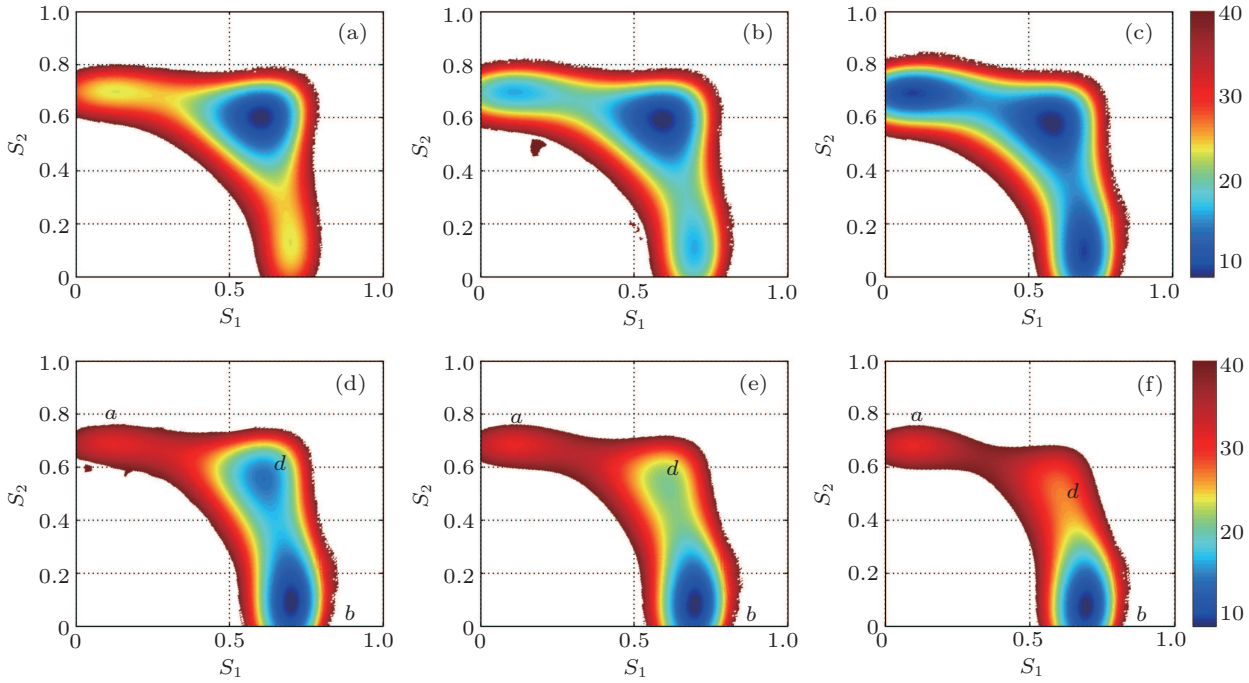


Fig. 11. (color online) Comparison of potential landscapes of different input thresholds for large inputs. (a)–(c) The two-dimensional potential landscapes for different input thresholds at the zero coherence level, where the strength of stimulus $\mu_0 = 60$ Hz and parameter $b = 107.5$, 108, and 108.5, respectively. (d)–(f) The two-dimensional potential landscapes for biased input ($\mu_0 = 55$ Hz) and with coherence $c' = 0.06$ and parameter $b = 107.5$, 108, and 108.5, respectively. In all subgraphs, parameters $a = 269.5$ and $D = 3.6 \times 10^{-7}$.

4. Conclusions

Although the attractor ideas have been used to describe cognitive processes such as decision making, a quantitative description of attractor landscapes has not been completely given yet, particularly at the non-equilibrium level. Here, we developed a theoretical framework that has been shown to be successful in describing associative memory and circadian rhythm,[23] to quantify the landscape for decision making. Furthermore, we quantified the decision-making processes by the optimal paths from undecided attractor states to decided attractor states on the landscape. An advantage of our landscape theory is not only showing the locations of attractors, but also showing the weight or depth of the attractors. We can quantify the stability of the functional attractors with the corresponding escape time and barrier heights on the potential landscape. The escape time quantified by the mean first passage time MFPT can also be used to quantify the decision times important in decision-making processes. Differently from the traditional way to get reaction time and performance, here, our quantifications of these features avoid the time-consuming calculations of the statistics of the data. Based on the potential landscapes and the optimal paths, we provided quantitative explanations of the experimentally observed behaviors and explored the underlying mechanisms of the speed–accuracy–energy tradeoff and changes of mind in the decision processes.

Following the neural trajectories, previous research showed the correlation between the decision time and accuracy for decision tasks with varying difficulty (c').[15,16] However, the underlying intrinsic mechanisms of the tradeoffs among speed, accuracy, and particularly the energy cost in decision making have not been explored. Recent fMRI studies on the speed–accuracy tradeoff strongly suggest the brain implements speed emphasis through increasing the baseline activity of cortical integrator neurons. We quantitatively discussed two mechanisms in speed emphasis with our landscape approach: one is increasing the baseline directly through presenting additional excitatory input (cortical theory) and the other one is increasing the baseline indirectly by reducing the inhibitory control to the integrator neurons (striatal theory). Our results suggest that these two ways show similar properties in the speed–accuracy tradeoff; i.e., the speed is increased at the expense of lost accuracy and higher energy cost in unit time. However, our results predict the two theories can be distinguished by the total energy cost in the whole decision-making process. If varying the input threshold (striatal theory) is the main regulation mechanism in the speed–accuracy tradeoff, the energy cost increases monotonously with increasing accuracy and decreases monotonously with a decreasing decision time. When presenting additional input is the dominated mechanism of regulating the speed–accuracy tradeoff, the total energy cost does not change monotonically with an increasing additional input. There is an optimal total energy cost with near optimal fast speed at intermediate accuracy. In other words, reasonable but suboptimal accuracy and performance can be achieved with optimal energy cost and speed. Some of our predictions have been supported by the experimental recordings that showed that the BOLD signal increases

in faster decisions. The total energy cost in the whole decision process should be tested in future experiments, which might also help in the optimal design of decision-making with speed, accuracy, and energy cost. It should be noted that we used a reduced two-population model to describe the decision-making process. When adding more biological details to the neural work, such as basal ganglia and globus pallidus, which are associated with movements, we may uncover more detailed mechanisms in decision making through quantifying the corresponding potential landscape and kinetic paths.

We explored the mechanism of mind changes with our potential landscape approach and found that it may be closely associated with the new state that emerges when the large stimulus inputs are presented. We also gave a physical explanation of why changes from the wrong to the correct choice occur more frequently and why more changes occur at a low coherence level, as has been observed in the experiments. We found that although errors are more likely to be made for a shorter decision time, there will be more chances for changes to correct these errors.

Our approach provides a general way to investigate cognitive behaviors which are determined by neural networks and the corresponding mechanisms. We wish to apply our theory to more complicated systems in future studies, for example decision makings with multiple alternatives and decisions associated with memory retrieval.

Appendix A: Mean first passage time

The mean first passage time τ from any state to a given final state can be obtained by solving the following equation: $\boldsymbol{F}\cdot\boldsymbol{\nabla}\tau+\boldsymbol{\nabla}\cdot\boldsymbol{D}\cdot\boldsymbol{\nabla}\tau=-1$.[28] The boundary condition is taken as an absorbing boundary condition $\tau=0$ at the final state and reflecting boundary conditions $n\boldsymbol{\nabla}\tau=0$ for the outer boundary.

Therefore, the average decision time can be approximately quantified by the mean first passage time from undecided states to decided states without knowing the exact decision threshold. It is because the time to the decided state is quite shorter after the barrier is crossed, compared with the time of crossing the barrier between two basins of the undecided state and the decided state. There is no doubt that the decision threshold lies in the basin of the decided state.

Appendix B: Entropy production rate

For non-equilibrium neural network dynamics, the driving force can be decomposed into a gradient of the potential and a curl flux force as: $\boldsymbol{F}=-\boldsymbol{D}\boldsymbol{\nabla}U+\boldsymbol{J}_{\rm SS}/P_{\rm SS}$. The entropy production rate can be quantified as: EPR $=\int \mathrm{d}I(\boldsymbol{J}\cdot\boldsymbol{D}^{-1}\cdot\boldsymbol{J})/P$.[28]

Appendix C: Decision-making pathways through path integral

According to corresponding Langevin equations from the decision-making neural network, we can now express the dynamics with the probability of starting from initial state $\boldsymbol{I}_{\rm initial}$ at $t=0$ and end at the final state $\boldsymbol{I}_{\rm final}$ at time t, with conditional probability as

$$\begin{aligned}
&P(\boldsymbol{I}_{\rm final},t,\boldsymbol{I}_{\rm initial},0)\\
&=\int\mathcal{D}[\boldsymbol{I}(t)]\exp\left[-\int\mathrm{d}t\left(\frac{1}{2}\boldsymbol{\nabla}\cdot\boldsymbol{F}(\boldsymbol{I})\right.\right.\\
&+\left.\left.\frac{1}{4}(\mathrm{d}\boldsymbol{I}/\mathrm{d}t-\boldsymbol{F}(\boldsymbol{I}))\cdot\frac{1}{\boldsymbol{D}(\boldsymbol{I})}\cdot(\mathrm{d}\boldsymbol{I}/\mathrm{d}t-\boldsymbol{F}(\boldsymbol{I}))\right)\right]\\
&=\int\mathcal{D}[\boldsymbol{I}]\exp[-S(\boldsymbol{I})]\\
&=\int\mathcal{D}[\boldsymbol{I}]\exp[-\int L(\boldsymbol{I}(t))\mathrm{d}t]. \qquad (5)
\end{aligned}$$

Here, $L(\boldsymbol{I}(t))$ is called the Lagrangian and the $S(\boldsymbol{I})$ is the action function or the weight for each path connecting initial state to final state. The integration for $\mathcal{D}[\boldsymbol{I}(t)]$ represents the sum over all possible paths between $\boldsymbol{I}_{\rm initial}$ at $t=0$ and $\boldsymbol{I}_{\rm final}$ at time t. It is a remarkable fact that not every path gives the same contribution. Each path has exponential weight, so we can approximate the path integral with a dominant path. The contribution of the optimal path is greater than the other path, therefore, the sub-leading path contributions are always small and can be ignored. In general, we can minimize the action function and resolve out the dominant path. Once the dominant path is obtained, we can also substitute into the path integral formulation and calculate the probability evolution in time.[22,32]

All the calculations above are completed with the COMSOL software.

Appendix D: Supplementary results and discussion about different initial conditions

The conventional way of exploring the neural network dynamical systems is always following the dynamical trajectories of the time evolution of the system. In these approaches the results are often influenced by the initial conditions. However, following the single trajectories cannot easily capture the global properties of the systems, especially for complex nonlinear neural network systems with intrinsic and external fluctuations. In this work, we focused on the probabilistic evolution which is linear and can give the global nature of the stochastic dynamics. When the evolution time is long enough, the probability distributions in the state space do not change. This is the steady state and the steady state probability distribution $P_{\rm ss}$ satisfies $\mathrm{d}P_{\rm ss}/\mathrm{d}t=0$. By solving the corresponding Fokker–Planck equation, we can quantify the steady state probability distributions of the system in the state space. Then

we define the potential function $U = -\ln P_{ss}$. We should notice that the steady state probability in the state space is only determined by the system itself and not influenced by the initial conditions. Therefore, with different initial conditions, the probability evolutions may follow different routes but will eventually always settle down to the common steady state distribution. The corresponding quantified attractor landscape is also independent of the initial conditions.

In the following figures, we show the evolution of the negative logarithm of the probability ($-\ln P$) for three different initial conditions, where no stimulus inputs are presented and the motion coherence $c' = 0$. When the evolution time is long enough, we can get the steady state probability distributions and the corresponding potential landscape $U = -\ln P_{ss}$. As we discussed in the main text of our paper, there are three attractors coexisting which correspond to one decided state and two undecided states before the stimulus onset. In Fig. D1, we choose the initial condition with the states close to the undecided state having larger initial probabilities (lower potentials). This implies the system starts from the state which has only one decided state. We can see as the probability evolves three attractors emerge on the landscape. Then we show the initial condition focusing on one decided state. We can see in Fig. D2 the potential landscape corresponding to steady state probability distributions also has the same three attractors, although the evolution follows a different route.

We also try the initial condition that the initial probabilities of all the states in the plane are uniform. We reach the same potential landscape in Fig. D3 with a different evolution track. These figures show different initial conditions can reach the same steady state probability distributions and potential landscapes in our probabilistic description, taking different evolution paths.

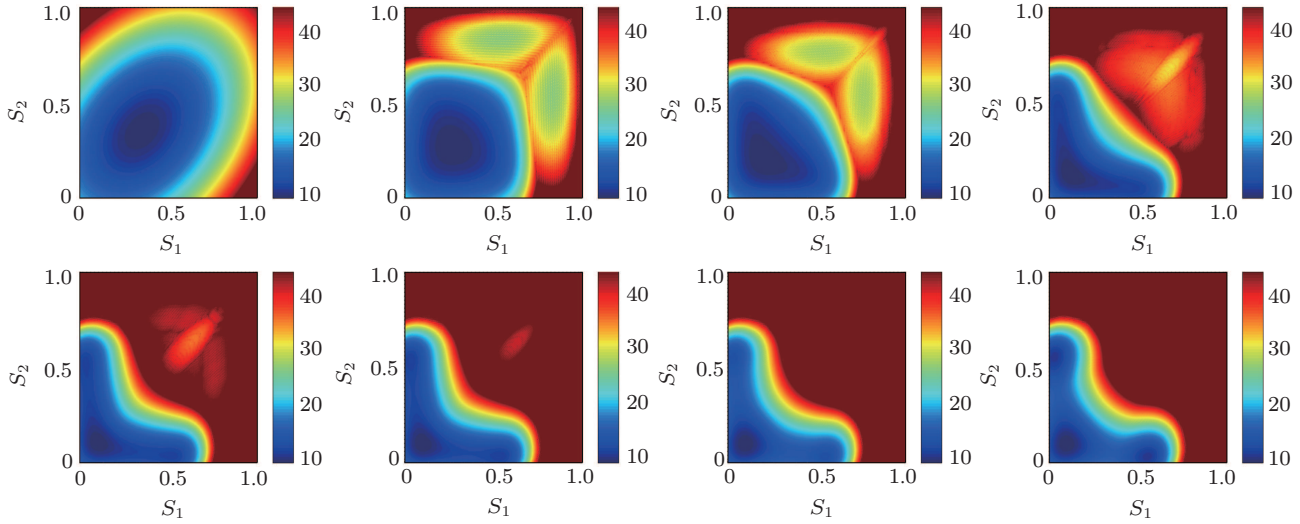


Fig. D1. (color online) Probability evolution and emergence of the tristable landscape with the initial condition focusing on the undecided state.

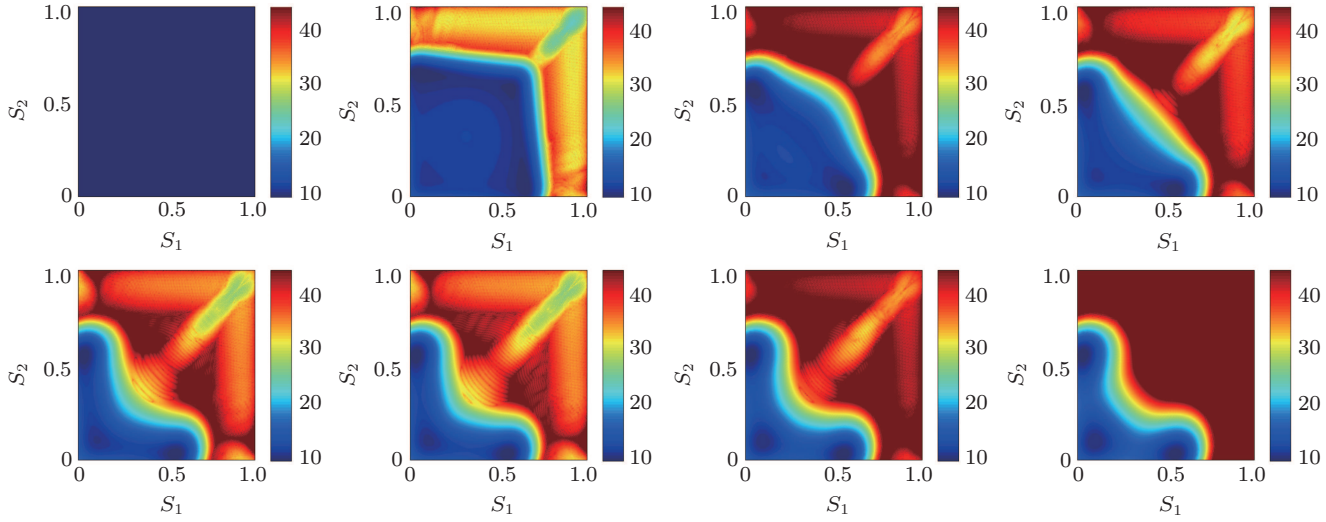


Fig. D2. (color online) Probability evolution and emergence of the tristable landscape with the initial condition focusing on one decided state.

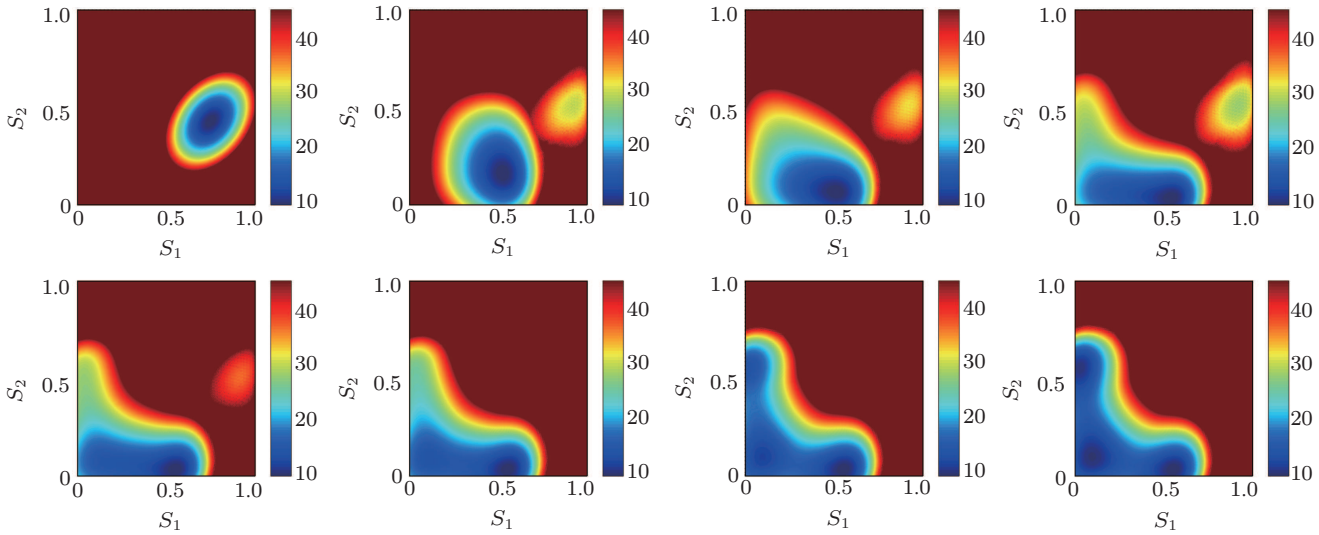


Fig. D3. (color online) Probability evolution and emergence of the tristable landscape with the uniform initial probability distribution.

With a path integral approach, we can quantify the weights of both the optimal decision paths in error trials and correct trials. Then we can quantify the ratio of correct responses in decision tasks. In our work, we defined the decision path as the one from the spontaneous undecided state to one of the two decided states, either the correct one or the incorrect one. On the quantified landscapes of the decision making network, there is a clear spontaneous undecided state. Our discussions about the decision time and performance (accuracy) are based on this spontaneous undecided state. Different initial conditions mean that the system starts from different initial states instead of the spontaneous undecided state. In fact, there is no difficulty to discuss the decision time and accuracy with our method for different starting points. We did not show these discussions in the main text because we believe setting the spontaneous undecided state as the starting point has a clearer biological meaning and is more appropriate.

Here we also show the landscapes for some different initial conditions at two different coherence levels ($c' = 0$ and $c' = 0.36$). In Fig. D4, we use the black dots to indicate the initial states and the white dots to indicate the final decided states. The blue lines represent the optimal paths from the initial state to the lower-right decided state (for biased motion coherence that c' is not zero, this state corresponds to the correct decided state). The pink lines represent the optimal paths from the initial state to the upper-left decided state in the error trials for non-zero coherence c'.

Then we calculated the accuracy (ratio of $P_{\text{correct}}/P_{\text{incorrect}}$) for different initial conditions, which are shown in Fig. D5. The x-coordinate 1, 2, and 3 correspond to the three initial conditions as shown in the above figure. When the motion coherence is unbiased ($c' = 0$), the ratio of the probabilities of two paths is equal to 1. For larger coherence c' (easier to make a decision), the accuracy of the decision task is always higher. However, we should notice that if the decision process from the initial state 2 in Fig. D4 (close to the incorrect decided state), it is likely to make an incorrect decision for lower motion coherence c' (ratio < 1). When the coherence c' is large enough, it is still likely to make the correct choice even though the initial state is close to the incorrect decided state.

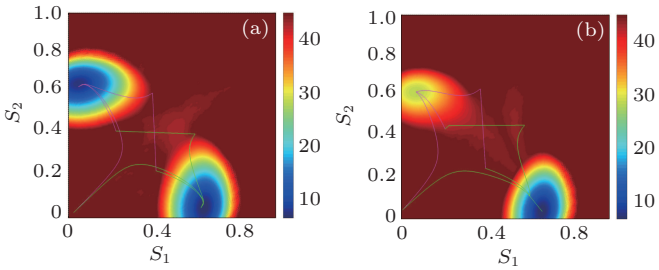


Fig. D4. (color online) Optimal decision paths for different initial states. (a) $c' = 0$; (b) $c' = 0.36$.

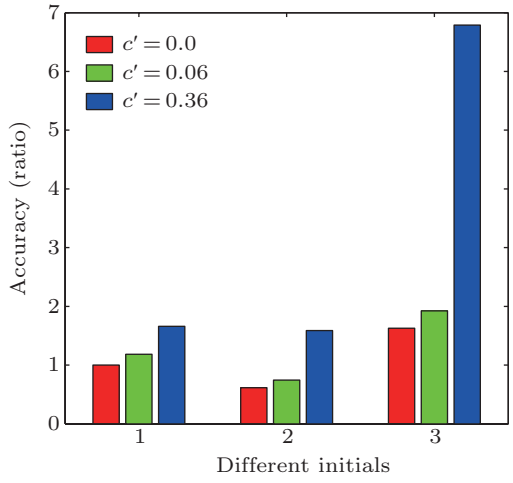


Fig. D5. (color online) The performance (accuracy) for different initial states.

References

[1] Abbott L F 2008 *Neuron* **60** 489
[2] Vogels T P, Rajan K and Abbott L F 2005 *Annu. Rev. Neurosci.* **28** 357
[3] Hopfield J J 1982 *Proc. Natl. Acad. Sci.-Biol.* **79** 2554
[4] Li Z P and Hertz J 2000 *Network-Comp. Neural.* **11** 83
[5] Mohr P N C, Biele G and Heekeren H R 2010 *J. Neurosci.* **30** 6613
[6] Churchland A K, Kiani R and Shadlen M N 2008 *Nat. Neurosci.* **11** 851
[7] Niwa M and Ditterich J 2008 *J. Neurosci.* **28** 4435
[8] Ratcliff R, Van Zandt T and McKoon G 1999 *Psychol. Rev.* **106** 261
[9] Gold J I and Shadlen M N 2007 *Annu. Rev. Neurosci.* **30** 535
[10] Wang X J 2008 *Neuron* **60** 215
[11] Roxin A and Ledberg A 2008 *PLoS Comput. Biol.* **4** e1000046
[12] Ratcliff R and Rouder J N 1998 *Psychological Science* **9** 347
[13] Shadlen M N and Newsome W T 2001 *J. Neurophysiol.* **86** 1916
[14] Wang X J 2002 *Neuron* **36** 955
[15] Wong K F and Wang X J 2006 *J. Neurosci.* **26** 1314
[16] Wong K F, Huk A C, Shadlen M N and Wang X J 2007 *Front. Comput. Neurosc.* **1** 6
[17] Li Z P and Dayan P 1999 *Network-Comp. Neural.* **10** 59
[18] Amit D J 1992 *Modeling Brain Function: The World of Attractor Neural Networks* (Cambridge: Cambridge University Press)
[19] Sasai M and Wolynes P G 2003 *Proc. Natl. Acad. Sci. USA* **100** 2374
[20] Wang J, Xu L and Wang E K 2008 *Proc. Natl. Acad. Sci. USA* **105** 12271
[21] Wang J, Li C H and Wang E K 2010 *Proc. Natl. Acad. Sci. USA* **107** 8195
[22] Wang J, Zhang K, Xu L and Wang E K 2011 *Proc. Natl. Acad. Sci. USA* **108** 8257
[23] Yan H, Zhao L, Hu L, Wang X D, Wang E K and Wang J 2013 *Proc. Natl. Acad. Sci. USA* **110** E4185
[24] Wang J 2015 *Adv. Phys.* **64** 1
[25] Xu L, Chu X K, Yan Z Q, Zheng X L, Zhang K, Zhang F, Yan H, Wu W and Wang J 2016 *Chin. Phys. B* **25** 016401
[26] Deco G and Marti D 2007 *Biol. Cybern.* **96** 487
[27] Deco G and Marti D 2007 *Phys. Rev. E* **75** 031913
[28] Zhang F, Xu L, Zhang K, Wang E K and Wang J 2012 *J. Chem. Phys.* **137** 065102
[29] Qian H 2009 *Method. Enzymol.* **467** 111
[30] Feng H and Wang J 2011 *J. Chem. Phys.* **135** 234511
[31] Xu L, Shi H, Feng H and Wang J 2012 *J. Chem. Phys.* **136** 165102
[32] Wang J, Zhang K and Wang E 2010 *J. Chem. Phys.* **133** 125103
[33] Elowitz M B, Levine A J Siggia E D and Swain P S 2002 *Science* **297** 1183
[34] Wang J, Xu L, Wang E K and Huang S 2010 *Biophys. J.* **99** 29
[35] Shadlen M N and Newsome W T 1996 *Proc. Natl. Acad. Sci. USA* **93** 628
[36] Roitman J D and Shadlen M N 2002 *J. Neurosci.* **22** 9475
[37] Huk A C and Shadlen M N 2005 *J. Neurosci.* **25** 10420
[38] Mazurek M E, Roitman J D, Ditterich J and Shadlen M N 2003 *Cereb. Cortex.* **13** 1257
[39] Resulaj A, Kiani R, Wolpert D M and Shadlen M N 2009 *Nature* **461** 263
[40] Waddington C H 1957 *The Strategy of the Genes* (London: London Pub)
[41] Wickelgren W A 1977 *Acta Psychol.* **41** 67
[42] Chittka L, Skorupski P and Raine N E 2009 *Trends. Ecol. Evol.* **24** 400
[43] Bogacz R, Wagenmakers E J, Forstmann B U and Nieuwenhuis S 2010 *Trends. Neurosci.* **33** 10
[44] Albantakis L and Deco G 2011 *PLoS Comput. Biol.* **7** e1002086
[45] Albantakis L, Branzi F M, Costa A and Deco G 2012 *Plos One* **7** e43131
[46] Ivanoff J, Branning P and Marois R 2008 *Plos One* **3** e2635
[47] van Veen V, Krug M K and Carter C S 2008 *J. Cognitive Neurosci.* **20** 1952
[48] Heitz R P and Schall J D 2012 *Neuron* **76** 616
[49] Forstmann B U, Dutilh G, Brown S, Neumann J, von Cramon D Y, Ridderinkhof K R and Wagenmaker E J 2008 *Proc. Natl. Acad. Sci. USA* **105** 17538
[50] Magistretti P J, Pellerin L, Rothman D L and Shulman R G 1999 *Science* **283** 496
[51] Binder J R, Liebenthal E, Possing E T, Medler D A and Ward B D 2004 *Nat. Neurosci.* **7** 295
[52] Heekeren H R, Marrett S and Ungerleider L G 2008 *Nat. Rev. Neurosci.* **9** 467